MULTISCALING AND MULTIFRACTALITY IN THE EARTH'S TOPOGRAPHY

by

Jean–Sébastien Gagnon

A thesis submitted to the Faculty of Graduate Studies and Research in partial fulfillment of the requirements for the degree Master in Science

Department of Physics

McGill University

Montréal, Canada

November 2001

ABSTRACT

Topographic transects coming from four different Digital Elevation Models (DEMs) which collectively span different ranges of scales from 20000 km to 0.5 m are analyzed. Power spectra, trace moments and structure functions are used to show that continents and oceans have the same moment scaling function K(q) but different (scale by scale) nonconservation H and also that the Earth's topography is multiscaling from planetary scales down to a few meters. The results also suggest that topography can be described statistically at all scales by a global K(q). The form of K(q) shows that the statistics of topography are close to those predicted by universal multifractals. It seems that the multiscaling of topography is broken because of the presence of trees on the DEM: they indroduce a characteristic length in the vertical that is approximately 9 m.

RÉSUMÉ

Plusieurs profils topographiques provenant de quatre Models de Terrain Digitaux (MTD) ayant des gammes d'échelles allant de 20000 km à 0.5 m sont analysés. Spectres de puissance, trace moments et fonctions de structures sont utilisés pour montrer que les continents et les océans ont la même fonction de "scaling" des moments K(q), mais des paramètres de non–conservation échelle par échelle H différents et que le relief terrestre est "multiscaling" sur une gamme d'échelle allant de l'échelle planétaire jusqu'à quelques mètres. Les résultats suggèrent aussi que la topographie peut être décrite statistiquement à toutes les échelles par une fonction K(q) global. Le multiscaling est brisé en raison de la présence d'arbres sur le MTD: ces derniers introduisent une échelle caractéristique verticale approximativement égale à 9 m.

AKNOWLEDGMENTS

In the course of my studies, I have been trough a lot of different situations and faced many problems. Alone, all those little things would have added up to the point where I would have completely broke down. But fortunately, I am surrounded with people that helped me reach my goal. To those people I am greatly indebted, and the least that I can do is thank them for their help. Here is a (non exhaustive) list of those people.

First, I thank my mentor, Prof. Shaun Lovejoy, for his advising and his patience with me. But more importantly, he taught me a method and helped me develop a critical mind towards physics, something that I will keep for the rest of my career. I thank the German Aerospace Center (DLR)'s Institute of Space Sensor Technology and Planetary Exploration for providing the high resolution DEM of Lower Saxony, which constitutes one of the main part of this study. Jean–Bernard Addor is also in my "line of fire" of thanks for helping me with those damned Linux computers, all the programming stuff and for fruitful discussions. Other thanks I give to Mehdi Talamali, Dominique Perrault–Joncas and Marc Lilley for discussions, atmosphere (in the lab) and all the things that I cannot recall.

Now, for my "other life" in UQAM, I thank the GEOTOP for financial support and their ressources. I especially thank Prof. Jean–Claude Mareschal for helping me finding references for the "geophysical" part of this study. I also thank the students (Evelise Bourlon, Chantal Gosselin and Stéphanie Nicopoulos to name but a few) for their friendship.

Finally, for my "real" life, I thank my dear Julie for much love and support.

CONTRIBUTION TO ORIGINAL KNOWLEDGE

Although multifractal analyses of topography have been done before, this thesis greatly extends the range of scales analyzed (planetary scales down to 0.5 m), which is larger then the previous studies by approximately 4 orders of magnitude. It is the first time that multiscaling is tested on so large a range of scales. Also, the quantity of data analyzed (in terms of number of pixels) ranges from $2x10^6$ to $2x10^8$, which is far larger than previous analyses.

An explicit comparison between continents and oceans is done for the first time, showing that they are similar at a certain statistical level but different at another level. Also, this thesis explicitly shows that the statistics of topography fluctuations are well described by a cascade process starting at planetary scales. The effect of trees on multiscaling is also studied for the first time.

TABLE OF CONTENTS

1. INTRODUCTION

1.1 Scaling in topography

In general, geological and geophysical fields are highly nonlinear and are extremely variable (in space and in time) over wide ranges of scales. More particularly, the field analyzed in this study, the Earth's topography, strongly varies from one place to another (i.e. there are large fluctuations) and from one scale to another, making them very elusive and hard to tackle.

One major breaktrough in the study of topography is the use of scaling ideas. Scaling is an interesting symmetry associated with power laws. If a system is described by a power law P(x), then the system is invariant under the change of scale $x \rightarrow \lambda^{-1}x$:

$$P(x)=x^S \quad \rightarrow \quad P(\lambda^{-1}x)=(\lambda^{-1}x)^S=\lambda^{-S}P(x) \tag{1.1}$$

This symmetry has a profound meaning. It means that analyzing a system at a particular scale is not so interesting: it is more useful to analyze how it changes with scales. Put it differently, it is the scale invariant exponent S that contains the important information in equ. (1.1) (the notion of scale invariance will be further discussed in section 2.2.1).

The study of power laws in topography has been and is still an active area of research. Half a century ago, Vening Meinesz (1951)[1] studied the spherical harmonics expansion of the Earth's topography of Prey (1922) and showed that the power spectrum of topography follows a power law with a

1 The original results are in Vening Meinesz (1951), but the essential points that are quoted here can be found in Heiskanen and Vening Meinesz (1958).

spectral exponent $\beta \approx 2$. After his pioneering work, others, like Balmino et al. (1973), made the same kind of study and confirmed his results. Bell (1975) used the spectra of his predecessors and added them to his own studies of abyssal hills to produce a composite power spectrum that is scaling over approximately 4 orders of magnitude with also a spectral exponent $\beta \approx 2$. Other more recent spectral studies (of bathymetry) with varying values of β in ranges going from 1000 km to 0.1 km can be found in Berkson and Matthews (1983) ($\beta \approx 1.6$–1.8), Fox and Hayes (1985) ($\beta \approx 2.5$) and Gibert and Courtillot (1987) ($\beta \approx 2.1$–2.3). There is also Sayles and Thomas (1978) who argued that many man made and natural surfaces (including the Earth's topography) exhibit scaling over 8 orders of magnitude with $\beta \approx 2$, but their results must be taken with care (Berry and Hannay (1978)) and will be discussed in section 5.1.

On the other hand, Herzfeld et al. (1995) and Herzfeld and Overbeck (1999) argue that the ocean floor (and topography in general) cannot be scaling over a wide range of scales, because of their conviction that geomorphologic processes are scale dependent (i.e. have characteristic lengths), meaning that they consider a priori that the scaling is necessarily broken. They show this by doing power spectra and variograms on single (short) transects and show that they are broken. But these results are not convincing, because scale invariance is a statistical symmetry (see section 2.2.1) that is almost surely broken on a single realization, so it is really important to have a lot of statistics to approximate the theoretically predicted ensemble scaling.

1.2 Simple scaling and monofractals

Richardson (1961) found that the length of a coastline varies with the length of the rulers used to measure it, and the form of this dependence is a

power law (see section 2.1.1). Mandelbrot (1967), in his famous article "How long is the coast of Britain", interpreted the scaling exponents of Richardson (1961) as being fractal dimensions. Later, with the avent of fractional Brownian motion (fBm) models of terrain (Mandelbrot (1975), Goodchild (1980)), many fractal studies on topography were made and some realistic simulations of topography were done. But as pointed out by Mark and Aronson (1984), because fBm is purely statistical in nature and is not based on geomorphic processes, this can only be an advance in computer graphics if it does not represent adequately "real" topography.

Since then, there has been many estimates of (supposedly unique) fractal dimensions on topographic transectss and surfaces using various methods to see if topography respects "fractal" statistics. Two commonly used methods are the power spectrum (see for example Gilbert (1989), Huang and Turcotte (1989, 1990)) and the variogram (see for example Burrough (1981), Mark and Aronson (1984)), where the fractal dimension D_f is related in a simple way to the spectral exponent $\beta=1+2H=5-2D_f$ (for transects) and to the variogram exponent $\xi=2H=4-2D_f$ (for transects). Another method, more commonly used in the study of interfaces, was also used by Dietler and Zhang (1992) to infer D_f from the roughening exponent χ via the relation $\chi=3-D_f$ (the roughnening exponent being equivalent to the Hurst exponent H only for strictly self–affine data). See Klinkenberg and Goodchild (1992), Xu et al. (1993) and Gallant et al. (1994) for reviews and discussions on the various methods used to infer the fractal dimension. But in general, neither spectra nor variograms can be used to infer fractal dimensions in this way, except by making very ad hoc monofractal hypotheses (for a discussion, see Lovejoy and Schertzer (1991)).

Direct estimates of the fractal dimension of topography and bathymetry (with the dividers method for example) are surprisingly rare (see for example Barenblatt et al. (1984), Aviles et al. (1987), Okubo and Aki (1987), Turcotte (1989)). Another direct procedure is to define sets of points (like iso–contours at a certain altitude threshold) and then compute D_f with a box–counting algorithm. For monofractal fields (like fBm), D_f is independent of the threshold (Falconer (1990)) but there is no reason that it should be the case in real topography (Lovejoy and Schertzer (1990)). An example of this is the case of a mountainous region with a really high mountain (singularity) in the middle. Calculating the box–counting dimension of the iso–contours at an altitude of 100 m will give a certain value, but the dimension of the iso–contours at an altitude near the summit of the highest mountain will certainly give a lower value. Lovejoy and Schertzer (1990) have shown with functional box–counting that D_f is indeed decreasing with increasing threshold, so it means that monofractals are at best an approximation of topography near the mean. The fractal geometry of sets seems to be insufficient to deal with all the variability (the extreme events like mountains) of the Earth's topography, so new tools are needed.

1.3 One step further: multiscaling and multifractals

There is only one fractal dimension (scaling exponent) associated with monofractals. But, as pointed out in section 1.2, one fractal dimension is not enough to describe topography: in fact, an infinity of fractal dimensions (one for each threshold) are needed to characterize a surface completely (Grassberger (1983), Hentschel and Procaccia (1983), Schertzer and Lovejoy (1983)). It is more appropriate to treat topography as a scale invariant field, which leads to the concepts of mathematical measures and multifractal fields (Parisi and Frisch (1985), Halsey et al. (1986), Schertzer and Lovejoy (1987), Meneveau and

Streenivasan (1987)). In multifractals, the unique scaling exponent (simple scaling) is replaced by a scaling function (multiscaling), which is infinitely more rich (each type of "singularity" has its own scaling exponent). Multifractal studies of topography that show that it is multiscaling in various regions of the world and over various ranges in scales can be found in Lovejoy and Schertzer (1990), Lavallée et al. (1993), Weissel et al. (1994), Lovejoy et al. (1995), Pecknold et al. (1997) and Tchiguirinskaia et al. (2000).

A recent article by Veneziano and Iacobellis (1999) points out that one of the methods used to demonstrate multiscaling in Lavallée et al. (1993), Lovejoy et al. (1995) and Pecknold et al. (1997) (i.e. taking the absolute value of the gradients before doing the trace moments analysis, see section 4.1.2) may produce spurious multiscaling. But as was already known, the break only occurs at the smallest scales and the method works well if this is taken into account. So, in the case of real topography with a large scale range, the problem is really small, if not totally inexistant. In any case, functional box–counting (Lovejoy and Schertzer (1990)) and generalized structure functions (Lavallé et al. (1993), Weissel et al. (1994)) also indicate multiscaling.

1.4 Physical models of topography

The natural topography of the Earth is very complex and its shape results from different processes, like tectonic forces (faulting, folding, flexure) and erosion, under the influence of gravity and other factors (Turcotte (1992), Lambeck (1988) and the references therein). The "equations" describing all topography are not known, but some models exist to explain certain features of topography. For example, the large swell around seamount chains can be explained by thermal expansion of the lithosphere caused by a heat source in

the mantle (hotspot, plume) (see Lambeck (1988)). Another important feature of topography is the bathymetry around mid–ocean ridges. Those ridges are sources of hot material coming from the mantle that create new oceanic crust (see for example Lambeck (1988)). The material injected at the ridge crest cools off, contracts and moves away as part of the plate, creating the characteristic topography that can be seen around those structures. In the framework of plate tectonics, two models were proposed to calculate the height of the terrain a certain distance away from the ridge: the thermal boundary layer model of Turcotte and Oxburgh (1967) and the plate model of McKenzie (1967) (see Parker and Oldenburg (1973) for a variant). The two models are similar (they rely on the equation of heat transport and isostatic equilibrium), but differ in their boundary conditions (Parsons and Sclater (1977)). Also, the thermal boundary layer model prescribes a mechanism that relates the surface observations to the flow in the mantle (i.e. convective cells that inject material at the ridge crest), which is not the case for the plate model. Both models predict that the height Δh of the topography after a certain time t, that can be converted into a distance l under the assumption of constant plate velocity, follows a power law of the form[2]

$$\Delta h \sim t^{-H} \phi' \sim l^{H} \phi \tag{1.2}$$

with H=1/2 and ϕ is a dimensional factor different for the two models. Those factors are

$$\phi = v_0^{\frac{-1}{2}} \left(\frac{\kappa \nu}{\alpha \Delta T g} \right)^{\frac{1}{3}} \quad and \quad v_0^{\frac{-1}{2}} \left(\frac{\rho_m \alpha \Delta T \kappa^{\frac{1}{2}}}{\Delta \rho} \right) \tag{1.3}$$

2 In fact, this power law is not so clear in the plate model, but Parsons and Sclater (1977) have shown that it is the case for times lesser than 70 M. years.

for the thermal boundary layer model and the plate model, respectively. The quantities are the velocity of the plate v_0, the thermal diffusivity κ, the coefficient of thermal expansion α, the temperature difference between the bottom and top plates ΔT, the acceleration of gravity g, the density of the mantle ρ_m and the density difference between mantle and seawater $\Delta\rho$. Sclater et al. (1971) have shown that the temporal dependence of equ. (1.2) is roughly respected in various oceans up to approximately 70 M. years[3].

The previous models of mid–ocean ridges are deterministic and are based on geomorphological equations. As can be seen from Turcotte and Oxburgh (1967) and McKenzie (1967), the general approach is to start with a set of highly nonlinear partial differential equations and simplify them (by making various assumptions and approximations) so that they can be solved. Those models are deterministic and do not predict the rugged aspect of sea–floor, i.e. they do not explain all the variability (Mareschal (1989)). They make important homogeneity hypotheses that reduce the problem to a few number of degrees of freedom. For example, in the thermal boundary layer model, under the length scale of a convective cell, everything in the mantle is considered to be "smooth".

To take into account the variability at all scales, there exists other approaches that are stochastic in nature. For example, Bell (1975) uses hills with random sizes that are uniformly distributed over the bottom of the ocean to model bathymetry (excluding mid–ocean ridges). The stochastic Kardar Parisi Zhang (KPZ) equation, introduced to study growing and eroding surfaces, is also used to model topography (see Dodds and Rothman (2000) for a pedagogical introduction). The latter approach uses scaling as a basic principle in addition to stochasticity. In fact, because the geomorphological equations

3 For times greater than 70 M. years, the relation becomes an exponential (Parsons and Sclater (1977)).

considered here are highly nonlinear, it is fruitful to consider one of the symmetries of the problem (i.e. scale invariance), which has been shown to hold in topography over various ranges (see section 1.1). Another stochastic approach based on scale invariance is the fractional Brownian motion model of topography of Mandelbrot (1975), that treats the height increments Δh as a random field rather than a deterministic quantity. The basic equation of this model can be written as

$$\Delta h_l = l^H \phi \tag{1.4}$$

where $\Delta h_l = h(\mathbf{x}+l\Delta\mathbf{x}) - h(\mathbf{x})$, $\mathbf{x}$ is a vector, $|\Delta\mathbf{x}|=1$, ϕ is a gaussian white noise with no scale dependence and $0<H<1$. If $H=1/2$, equ. (1.2) and (1.4) are similar, meaning that the latter can be thought as a stochastic version of the former (Lovejoy et al. (1995)). The fBm model gives realistic simulations of topography that reproduces its rugged aspect, but the problem is that it is a monofractal, which makes it less suitable to model a highly variable field like topography (see section 1.3).

A multifractal version of equ. (1.4) is simply obtained by replacing the scale independent noise with a scale dependent multifractal noise ϕ_l (Lovejoy et al. (1995)). This multifractal noise, called a (topographic) flux, is the result of a cascade process (see sections 2.2.1 and 2.3.3), which is a scale invariant random multiplicative mechanism. In the spirit of Turcotte and Oxburgh (1967) and their convective cells (with a characteristic size), the cascade means that there are all sorts of cells with different sizes, giving rise to altitude power laws at all scales. So, the highly nonlinear but scaling dynamics of the mantle lead to spatial fluctuations in the heat flux, and those fluctuations are converted into altitude fluctuations via thermal expansion. With dimensional analysis, it is

possible to find an expression for the topographic flux which is in agreement with the simple physics above and the value H=1/2 (Lovejoy et al. (1995)):

$$\phi_l \approx \left(\kappa \left(\frac{\rho}{Q_l} \right)^{\frac{1}{3}} \right)^{\frac{1}{2}} \tag{1.5}$$

where ρ is the mean density, Q_l is the multifractal heat flux and κ is the mean thermal diffusivity[4]. Equations (1.3) and (1.5) are not the same because they do not incorporate exactly the same physics. Although strictly speaking equ. (1.5) is for oceans, an analogous flux has been proposed for continents by Lovejoy et al. (1995). Considering that the standard orographic models assume plate collisions and isostatic equilibrium coupled with continental erosion, the most basic dimensional quantities responsible for the altitude fluctuations are

$$\phi_l \approx \frac{\Delta v_l}{\sqrt{g}} \tag{1.6}$$

where Δv_l is the horizontal velocity field of the tectonic plates and g is the acceleration of gravity (here again H is assumed to be 1/2). Of course, those dimensional analyses (equ. (1.5) and (1.6)) are very simple, but they give an idea of the physics of the problem. The advantage is that they do not make homogeneity hypotheses, i.e. they take all the variability into account.

4 Other combinations can be obtained by adding other dimensional quantities, but none are more justified than the other. More knowlegde about the system would be necessary to make a choice.

1.5 Objectives of the present study

As pointed out in the previous sections, topography seems to be scaling over various ranges of scales. Monofractals are not appropriate for studying topography because of its high variability, and the neglect of variability at smaller scales is also a fundamental weakness in the deterministic models of Turcotte and Oxburgh (1967) and McKenzie (1967). So the framework that is used in this study (described in chapter 2) is the multifractal framework based on cascades of Schertzer and Lovejoy (1987, 1991).

Because scale invariance (scaling) is fundamental in the cascade model, one of the important point of this study is to verify if topography is (multi) scaling over a wide range of scales by using different methods, following Lavallée et al. (1993), Lovejoy et al. (1995) and Pecknold et al. (1997). In fact, the range covered in this study goes from planetary scales down to 0.5 m, which is 4 orders of magnitude greater than the ones used in the previous studies. Also, the quantity of data (in terms of number of pixels) analyzed in this study is between $2x10^6$ and $2x10^8$ (depending on the data set), which is far larger than the previous multifractal analyses (where the number of pixels used is less than 10^6).

This huge range of scales and this vast amount of data allow the verification of three hypotheses. The first one concerns the difference between continents and oceans. Continents and oceans do not have the same geological history, meaning that their topography are probably the result of different processes. For example, the erosion on continents has been due to water (under the influence of gravity), wind and glaciers, whether in the oceans it has probably been due to marine currents. This means that there is probably a

difference in the statistical parameters describing the topography of continents and oceans. In the case of clouds observed over continents and oceans, it is mentioned in Lovejoy et al. (2001) that the only statistical parameter (describing the texture of the clouds) different in the two groups is H; the universal parameters α and C_1 are similar (see section 2.3.3 for details about those parameters). So, in the spirit of Lovejoy et al. (2001), it is expected that the only difference between topography of continents and oceans is in their H parameter.

The second hypothesis is about the multiscaling and the "global" properties of topography. More precisely, the large range of scales of this study allows to verify if topography is multiscaling and if there is an underlying mechanism that can describe topography at all scales. The specific mechanism discussed in this study is the cascade (see sections 1.4 and 2.2.1 for more details). This is the simplest hypothesis that can be made about the Earth's topography. It is important to point out that different geomorphological processes (like crust generation and erosion) generate anisotropies, but these anisotropies are not taken into account in this study. The analyses are defined isotropically, which means that anisotropies are largely washed out and do not enter in the present discussion of the global underlying mechanism of topography.

An analysis of the multiscaling of topography to such a high resolution (i.e. 0.5 m) can lead to problems. At this resolution, small structures like trees are resolved and enter the analysis. Because they are not part of the "natural" topography, those structures are expected to affect the statistics of topography in some way. So, the third hypothesis is that the presence of trees on a DEM can break the (multi) scaling of topography at small scales.

2. THEORY

2.1 Basic definitions

2.1.1 Intuitive idea of fractal dimension

The notion of fractal dimension (more usefully the codimension) is important in the theory of multifractals. To clarify this concept, consider the measurement of the length of a coastline with a ruler of length l (Richardson (1961)). It takes a certain number of rulers N(l) to cover all the coastline. If the length of the ruler is decreased, then N(l) increases, because with smaller rulers, it is possible to catch more details. Richardson empirically found that the number of rulers needed to cover the coastline follows a power law of the form

$$N(l) \sim l^{-D_f} \tag{2.1}$$

where D_f is an exponent that does not vary with l. Of course, this exponent is invariant only over a certain range of l: for l larger than the coastline, it will take only a "fraction" of a ruler to cover it and for l smaller than the smallest structure of the coastline (say a grain of sand, which is some sort of characterisic length), than no more details will be added by taking smaller rulers. Mandelbrot (1967) interpreted this exponent as the fractal dimension of the coastline. Except for smooth curves, D_f is usually fractional, hence the name "fractal". Also, because equ. (2.1) is a power law, the length of the coastline is scaling, where the fractal dimension D_f is a scale invariant exponent. In fact, the fractal dimension is just a special case of the more general class of scale invariant exponents.

2.1.2 The statistical codimension as a scaling exponent

The definition of the geometrical codimension of a set A is $C_g(A) = D - D_f(A)$ where $D_f(A)$ is the fractal dimension of the set A and D is the dimension of the embedding space E. By definition $0<C_g(A)<D$, so $C_g(A)$ is in fact bounded because it is defined on compact sets. In the multifractal formalism used in this study, one deals with statistics rather than geometry, so it is important to extend the definition of geometrical codimension and give it in statistical terms.

To see how to define the statisitical codimension, let's start with the probability that a set A is intersected by balls of diameter l. Because a probability can be interpreted as a frequency, then it is equal to the number of balls intersecting A divided by the number of balls intersecting E:

$$Pr(B_l \cap A) = \frac{N(B_l \cap A)}{N(B_l \cap E)} \tag{2.2}$$

Because this equation is just like counting a certain number of events with a certain "ruler" (ball) of size l, then it is similar to equ. (2.1), so we can write:

$$Pr(B_l \cap A) \sim \frac{l^{-D_f(A)}}{l^{-D}} = l^{C_g(A)} \tag{2.3}$$

The geometrical codimension is recovered in this way. But it is even more useful to define the statistical codimension with equ. (2.3) (removing the subscript g), or by saying that it is the scaling exponent of the measure of the fraction of the space occupied by the set A. Define in this way, it can be applied to random sets. Also, it doesn't have to be define on compact sets: E can be an infinite probability space. In practice, for example, when studying a two

dimensional topographic image, each pixel can be considered as the result of some random process, and by adding images, we add more pixels and we increase the portion of probability space that is explored. This allows the possibility of studying extreme events (such as very high mountains) that are almost surely not present on one sample, but will almost surely be present given enough samples.

2.2 Multiplicative processes and multifractals

2.2.1 Cascades and scale invariance

The phenomenological model behind the multifractal formalism used in this study comes from turbulence and his represented by a cascade. It was introduced to "explain" the intermittency of turbulence, i.e. the possibly large statistical fluctuations (in space and time) of the energy flux on each realization. The cascade model is motivated by the following properties that can be derived from the Navier–Stokes equations:

1) There is a conserved quantity, the energy flux ε, that is conserved by the nonlinear terms of the Navier–Stokes equations.

2) The Navier–Stokes equations are invariant under the change $\mathbf{x} \rightarrow \mathbf{x}/\lambda$, $\mathbf{v} \rightarrow \mathbf{v}/\lambda^S$, $t \rightarrow t/\lambda^{1-S}$, $\nu \rightarrow \nu/\lambda^{1+S}$, $\mathbf{F} \rightarrow \mathbf{F}/\lambda^{2S-1}$, where $\lambda=L/l$ is the ratio of the largest scale L of the system and the scale of observation l and S is an arbitrary scaling exponent, i.e. the equations are scale invariant. This means that, in principle, the solutions can be also scale invariant. Note: In this change of variable, the viscosity at one scale is different from the viscosity at another scale. Because the viscosity is fixed in a fluid, there is a problem in the application of the result to

real systems. It is one of the reason why this model is only expected to be exactly valid in the limit where the Reynold number is infinite (or the viscosity tends to zero). So the scaling should be respected in a certain range, called the inertial range: between the inner scale l_{inner} (under which viscosity becomes important) and the outer scale L_{outer} (where the energy enters the system).

3) The Navier–Stokes equations are local in Fourier space, meaning that structures (in turbulence, eddies) of a certain size interact most strongly with structures of similar sizes. It can be proved that a system having a spectrum that is a power law is local if the spectral exponent is $1<\beta<3$.

The multiplicative cascade model is based on these three ingredients. In our atmosphere, the solar forcing injects energy at the planetary scale and creates large eddies. Because of nonlinear interactions, those eddies break down into smaller eddies (but with size not too different from the original ones), and so on to the inner scale where the eddies are dissipated (typically 1 mm). At each scale, the ensemble average of the energy flux is conserved and it must be transmitted in a scale invariant way. In other words, it means that the energy at the largest scale is modulated by nonlinear interactions as it goes down the scales, giving a signal that looks very spiky at the smallest scale. In this model, all the nonlinear interactions are degrees of freedom (there are an infinite number of them) represented by random variables with a certain distribution and the problem is dealt with statistically. See Lovejoy et al. (2001) for a direct confirmation of the cascade model in clouds.

As it will be shown in section 2.2.3, multifractals are the generic result of cascades. The motivation behind cascades comes from turbulence, but like thermodynamics, which holds independently of its microscopic counterpart (i.e. statistical mechanics), it can be applied to other systems (including topography)

if the fundamental assumption of scale invariance is respected[5]. This is why scale invariance is an important symmetry and is at the base of this study: highly nonlinear problems with a very large number of degrees of freedom are very hard to tackle, so if this symmetry is respected, then it is possible to exploit it so that the problem becomes manageable. A word about "respected" is important here. Because cascades are stochastic processes, the quantities studied are statistical in nature and one must look at their statistical properties (like their average for example). Scale invariance is a statistical symmetry defined on an infinite ensemble, so that it is almost surely broken on a single realization. It is important to look at the average of many realizations of a process to observe good scaling.

2.2.2 The β–model

According to the previous section, the nonlinear interactions modulate the flux from one scale to another. This modulation of the flux is modeled by random multiplicative increments that multiply the flux. To visualize the cascade (in 2–D, so that it is easy to compare it to a topographic surface), let's consider a surface of size L and an elementary scale ratio λ (that is usually taken to be 2 in the case of discrete cascades). After one step, the surface is divided into squares of size $l_1 = L/\lambda_1$, and the flux ϕ in each square is multiplied by a different random multiplicative increments μ. After n steps, the flux in each square of size $l_n = L/\lambda^n$ is the result of a multiplication of many random increments. An important question here is to know what is the probability distribution of the increments (i.e. how they modulate the flux). The simplest

5 From now on, the "flux" ϕ will mean any conserved quantity that is cascaded down the scales, which is the energy per unit mass ε in the case of turbulence but can be different for other systems. Also, "eddies" in turbulence will be replaced by the more general term "structures".

multiplicative process imaginable is the β–model (see Monin and Yaglom (1975) and the original references therein), which is a simple binary (dead or alive) process defined as

$$Pr(\mu=\lambda^{c})=\lambda^{-c}$$
$$Pr(\mu=0)=1-\mu^{-c} \qquad (2.4)$$

where Pr(x) denotes the probability associated with a certain event x, μ is a multiplicative increment, c is the codimension of the space occupied by the nonzero flux set and $\lambda = L/l$ is the ratio of scales. The multiplicative increments are chosen so that the flux is conserved on average, i.e. $\langle\phi\rangle = 1$ or equivalently $\langle\mu\rangle = 1$. In words, equ. (2.4) means that the probability that a structure of scale l remains "alive" depends on the fraction of the space (see section 2.1.2) occupied by the "alive" structures. After n steps, the probabilities become

$$Pr(\phi_n=(\lambda^{n})^{c})=(\lambda^{n})^{-c}$$
$$Pr(\phi_n=0)=1-(\lambda^{n})^{-c} \qquad (2.5)$$

where ϕ_0 is taken to be 1 (without loss of generality). The resulting set of nonzero flux is a random fractal with a unique fractal dimension. This model gives some intuition about cascades but is too simplistic to completely characterize topography, because it is characterized by only one fractal dimension (see section 1.2 for more details).

2.2.3 The α–model

The α–model (Schertzer and Lovejoy (1983)) was introduced to show that the β–model was highly singular with respect to the generic cascade process. In fact, it is the simplest perturbation of the latter: instead of having a dead/alive binary process, it is a decrease/increase binary process where the probability distribution of the multiplicative increments is

$$Pr(\phi=\lambda^{\gamma_1})=\lambda^{-c}$$
$$Pr(\phi=\lambda^{\gamma_2})=1-\lambda^{-c} \qquad (2.6)$$

where $\gamma_1>0$ and $\gamma_2<0$ are pure orders of singularity and, as before, the ensemble average is conserved. It is easy to understand that after n steps, the succession of decreases/increases leads to a complexification of the flux. In fact, it leads to a whole hierarchy of singularities γ_i having different values (it gives shades of grey instead of a black and white flux as in the β–model). The cascade just described is discrete, but it is possible to let the scale ratio tend to a continuous limit (there are no a priori quantification rules, like in quantum mechanics), giving rise to a continuum of singularities γ. With this hypothesis and by taking the limit $\lambda \to \infty$ (the small scale limit), the cascade defined by equ. (2.6) implies (Schertzer and Lovejoy (1987, 1991))

$$Pr(\phi_\lambda \geq \lambda^{\gamma}) \sim \lambda^{-c(\gamma)} \qquad (2.7)$$

where ϕ_λ is the flux at scale L/λ, λ^γ is the threshold corresponding to the singularity γ and $c(\gamma)$ is a nonlinear convex function called the codimension function. The proportionality sign includes factors that vary slowly with λ.

Refering to equ. (2.3), equ. (2.7) means that the set defined by the condition $\phi_\lambda \geq \lambda^\gamma$ has a (fractal) codimension given by $c(\gamma)$ (see Fig. 2.1). So the flux is composed of a hierarchy of interwoven sets, one for each threshold, which have different fractal codimensions: a multifractal.

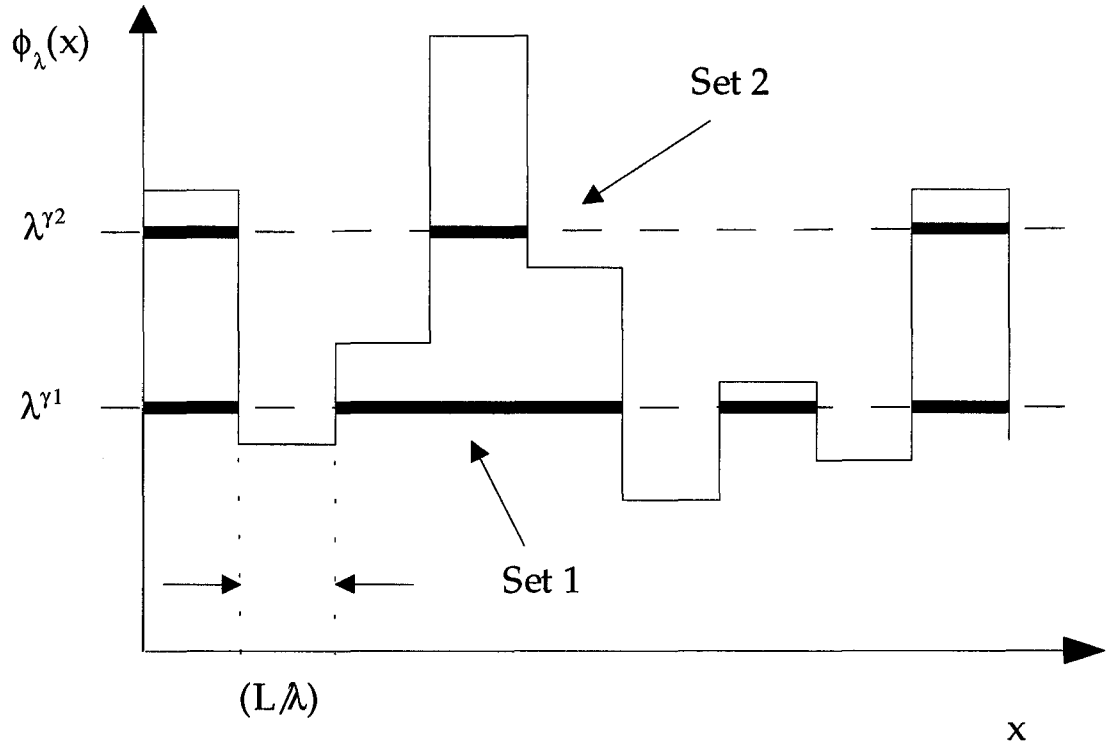

FIG. 2.1. Illustration of the α–model. For different thresholds $T_1=\lambda^{\gamma 1}$ and $T_2=\lambda^{\gamma 2}$ (with $\gamma_2>\gamma_1$, implying $T_2>T_1$), the corresponding sets (defined by $\phi_\lambda>T$) have different fractal dimensions (with $D_f(\gamma_2)<D_f(\gamma_1)$) or fractal codimensions ($c(\gamma_2)>c(\gamma_1)$).

2.3 Universal multifractals

2.3.1 The moment scaling function K(q)

In section 2.2.3, it was shown that c(γ) is the scaling exponent of the probability distribution of the flux values. In statistics, in it known that a random variable can be specified by its probability distribution or by all its statistical moments. So, it can be shown (Schertzer and Lovejoy (1987, 1991)) that the flux (which is a random variable) can also be described (in the small scale limit) by

$$\langle \phi_\lambda^q \rangle = \lambda^{K(q)} \tag{2.8}$$

where q is the order of the moment and K(q) is a nonlinear convex function called the moment scaling function. If the flux is conserved (i.e. $<\phi_\lambda>=1$), then it implies that K(1)=0 (K(0) is also equal to zero, trivially). Equations (2.7) and (2.8) are completely equivalent, and c(γ) and K(q) are related via a Legendre transform:

$$K(q) = \max_\gamma (q\gamma - c(\gamma)) \tag{2.9}$$

K(q) is the function that characterizes the scaling of the moments of the flux, hence its name. There is a one–to–one correspondence between the γ's and the q's and this can be seen in the following way. The l.h.s of equ. (2.9) means that we take the q^{th} power of the flux (degraded at a certain resolution λ) and then average over all the flux. If we take a low q (<0), all the large singularities (high γ) are smashed down, so the average is dominated by the small singularities

(low γ), which are more numerous (due to the convexity of $c(\gamma)$). If we take a large q (>0), then the difference between the low singularities and the high singularities will be even more pronounced, so the few high singularities will dominate the average. It means that the use of a certain value of q allows the analysis of a certain type of singularity γ.

2.3.2 Universality

The notion of universality is basic in physics. It is the property that says that the parameters of the theoretical model of a certain phenomenon are not all relevant: no matter what are the details of the model, the behavior of the system will be the same. In physics, universality is mostly known in the context of the renormalization group (see for example Wilson (1979)). Other examples of universality are the Feigenbaum constants of period doubling (see Strogatz (1994) for an intuitive introduction). He showed that those constants (which are related to the rate of convergence at which there is period doubling in unimodal maps) are universal, meaning that they don't depend on what is the exact form of the map: the only important "detail" to consider is that the map must have a quadratic maximum.

Other important examples of universality arise in the asymptotic description of sums of random variables: the central limit theorem (see for example Feller (1971)). In its most familiar form, it says that the sum of many independent random variables having (possibly) different distributions with a finite variance gives a random variable having a gaussian distribution. The gaussian distribution is some sort of stable attractor: no matter what are the "details", it necessarily gives a gaussian. More generally, if the finite variance restriction is relaxed, then the resulting attractor is called a stable distribution

(see for example Samorodnitsky and Taqqu (1994) or Uchaikin and Zolotarev (1999) for good treatments), which has the gaussian distribution as a special case.

Returning to the problem of multifractals and the moment scaling function K(q) needed to characterize them, the only constraint on this function is that it must be convex. So it means that an infinite number of parameters could be used to describe it, which is not really useful. But universality tells us that there is a possibility that only a few of these parameters are relevant. Schertzer and Lovejoy (1987, 1991) showed that there is universality in multifractal processes (see Schertzer and Lovejoy (1997)) for the debate about this issue). The point is that multifractals are the generic result of multiplicative cascade processes: each section of the flux is the result of a multiplication of many random increments. This process can be turned into an additive process by taking the logarithm of the random increments: this gives a sum of random variables, and all the question is about the stability of this sum. Schertzer and Lovejoy (1987, 1991) showed that if the process is continuous in scales and if the probability distribution of the multiplicative increments is logstable (with maximum asymmetry), then the universal functional form for K(q) is given by

$$K(q)=\frac{C_1}{\alpha-1}(q^{\alpha}-q) \tag{2.10}$$

where α is the index of stability related to the distribution ($0\leqslant\alpha\leqslant2$) and C_1 is the codimension of the singularity that contributes the most to the mean of the process. The case $\alpha=0$ corresponds to the β–model of section 2.2.2 and the case $\alpha=2$ corresponds to the lognormal model (see Monin and Yaglom (1975) and the original references therein), so α can be seen as a degree of deviation from

monofractality. Also, when $C_1=0$, it means that the set corresponding to q=1 is space filling, so it can be interpreted as a deviation from homogeneity.

2.3.3 Fractionally Integrated Flux model

In turbulence, the energy flux ε is not directly observable, it is the velocity shear that is measured. If we consider an eddy (structure) of size $l=L/\lambda$ and suppose that there is no intermittency (there are no fluctuations in the energy flux), then the difference in velocity (shear) between opposite ends of the eddy follows Kolmogorov's law

$$\Delta v_\lambda \sim \lambda^{-H} \epsilon_\lambda^a \tag{2.11}$$

where H=1/3 and a=1/3 (by dimensional analysis). To take intermittency into account (possible scale dependent large fluctuations in ε), then the constant ε in equ. (2.11) must be replaced by a multifractal energy flux that allows large fluctuations. Then, the λ^{-H} term fractionally integrates the multifractal noise, i.e. makes some sort of smoothing. This fractional integration can be seen as a power law filter of order H in Fourier space.

In section 2.2.1, it was mentioned that cascades are used to model turbulence, but that if scale invariance is respected, then the model can be applied to other systems as well. So the model used in this study to characterize topography is based on an equation similar to equ. (2.11):

$$\Delta h_\lambda = \lambda^{-H} \phi_\lambda \tag{2.12}$$

where $\Delta h_\lambda = h(\mathbf{x}+\lambda^{-1}\Delta\mathbf{x}) - h(\mathbf{x})$ (with $L=|\Delta\mathbf{x}|$) are the height fluctuations a distance

$l=L/\lambda$ apart, ϕ_λ is a multifractal "topographic" flux (resulting from a multiplicative cascade process) and H is the Hurst exponent. This model is called the Fractionally Integrated Flux (FIF) model. See section 1.4 for the physics of the problem and for a discussion of H=1/2 in topography.

We can look at the moments of equ. (2.12) by taking the q^{th} power on both sides and then taking the ensemble average, which leads to

$$\langle|\Delta h_\lambda|^q\rangle=\lambda^{-qH}\lambda^{K(q)} \tag{2.13}$$

where $\langle\phi_\lambda{}^q\rangle=\lambda^{K(q)}$ (see equation (2.8)) and K(q) is given by equ. (2.10). H can be seen as the degree of non–conservation of the mean of the process with scale. If, in equ. (2.12), ϕ_λ is a scale independent noise (like gaussian white noise in the case of fBm) instead of a scale dependent multifractal noise, then no $\lambda^{K(q)}$ would appear in equ. (2.13). This means that in the case of simple scaling K(q)=0, or that multiscaling implies a nonzero K(q).

3. DATA SETS

In this study, different Digital Elevation Models (DEMs) that span various ranges of scales are analyzed. DEMs are gridded representations of topography. They are constructed via various techniques like stereo–photography and in situ measurements of altitude, put together (often using interpolation schemes) and then gridded so as to obtain a height pixel field. They are essentially characterized by two numbers: their horizontal resolution and their vertical resolution.

Because of their method of construction and the gridding, DEMs can have some problems (see Weissel et al. (1994) for an example), one of them being the insufficient dynamical range. The dynamical range is related to the number of different values the height measures can take (it is related to the vertical quantization). For example, measuring the height of a mountain with a ruler of 1 km does not give many different values (maybe 2 or 3, depending on the mountain): there are much more variations if it is a 1 m ruler. So an insufficient dynamical range means that there is frequently not much pixel to pixel variability in the height measurements, the surface is not well represented and looks too smooth. Another problem can be the oversampling, i.e. measurements of altitude in some regions are probably more distant than the resolution of the DEM, but to have a regular grid of constant resolution, they interpolate between them, an operation that artificially smooths the DEM.

Four different DEMs are analyzed in this study (see table 3.1 for their individual characteristics):

1) ETOPO5: Global topography and bathymetry (see Fig. 3.1) (Data Announcement 88–MGG–02, Digital relief of the Surface of the Earth. NOAA, National Geophysical Data Center, Boulder, Colorado, 1988)

2) GTOPO30: Global continental topography (see Fig. 3.2 for the U.S. part) (http://edcdaac.usgs.gov/gtopo30/README.html).

3) United States: DEM of the United States (U. S. Geological Survey)

4) Lower Saxony: DEM of a 3 km x 3 km section of Lower Saxony (see Fig. 3.3) that was constructed with the help of the HRSC–A (High Resolution Stereo Camera Airborn) (Wewel et al. (2000)).

Data sets	*Horizontal resolution*	*Vertical quantization*	*Number of transects analyzed*	*Length of transects (km)*
ETOPO5	5′ (≈10 km)	1 m	500	40000
GTOPO30	30 ″ (≈1 km)	1 m	1225	4096
U.S.	90 m	1 m	2500	5898
Lower Saxony	50 cm	10 cm	3000 (or 500*)	3 (or 0.512*)

* Treeless part

TABLE 3.1. Table showing the different characteristics of the DEMs studied. Also shown are the number of transects (with their length) analyzed in each DEM (see sections 4.2.2 and 4.2.3).

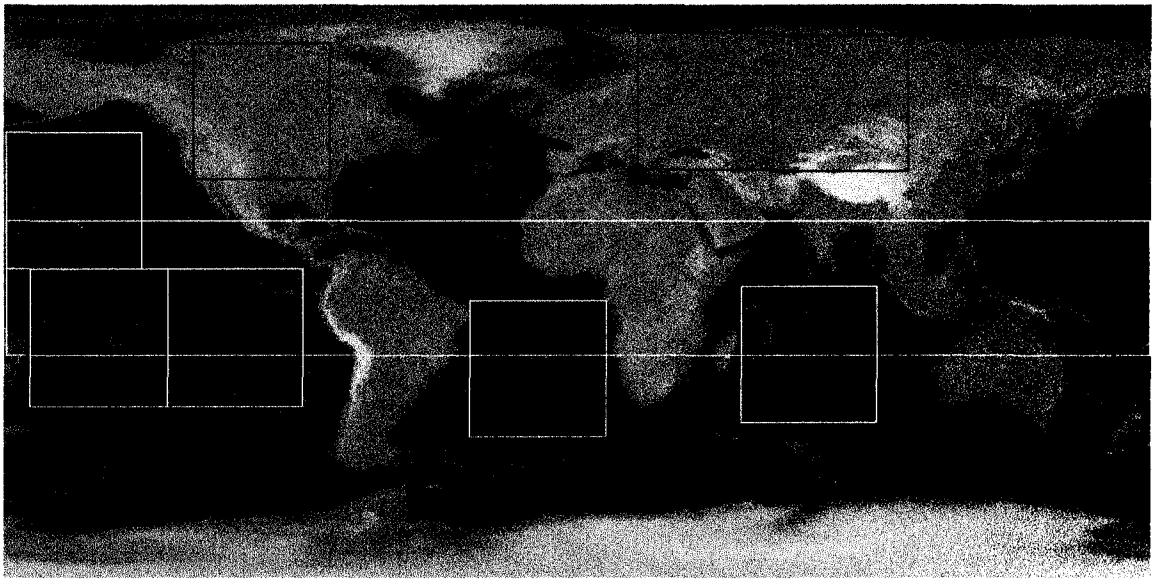

FIG. 3.1. ETOPO5 data set. The white and black squares indicate the areas studied in section 4.2.1. The white rectangle indicates the area studied in section 4.2.2 (500 transects of 40000 km).

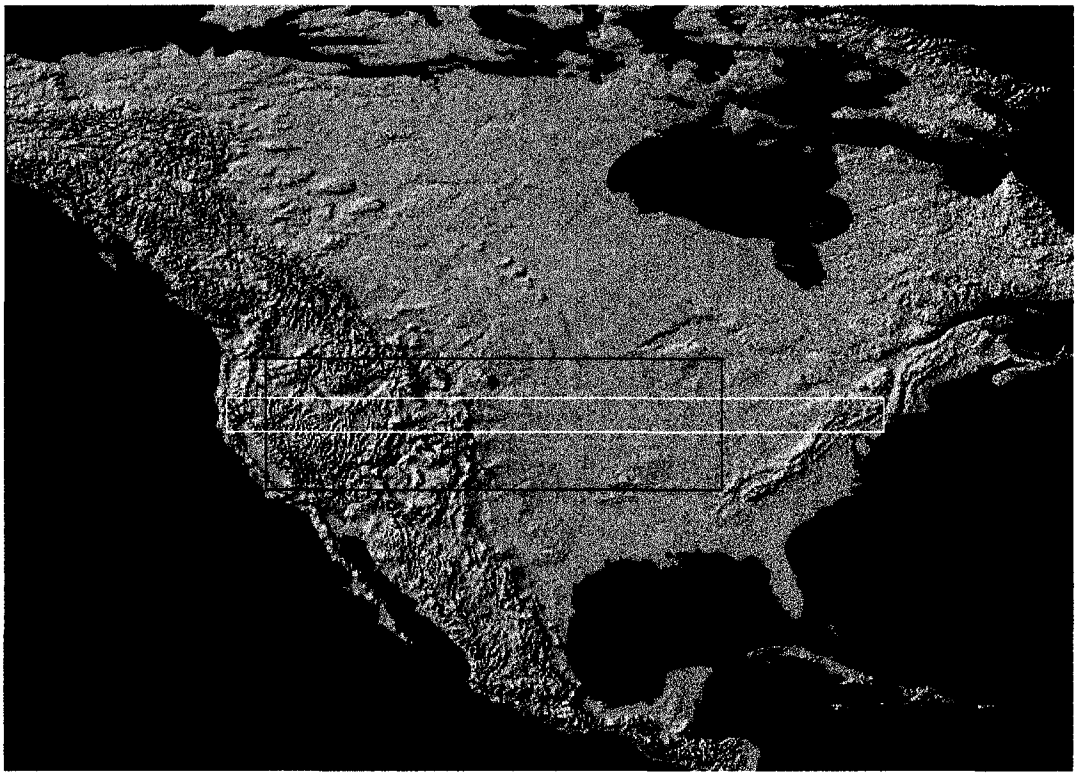

FIG. 3.2. U.S. part of the GTOPO30 data set. The black rectangle indicates the area studied on GTOPO30 (1225 transects of 4096 km) and the white rectangle indicates the area studied on the U.S. DEM (2500 transects of 5898 km).

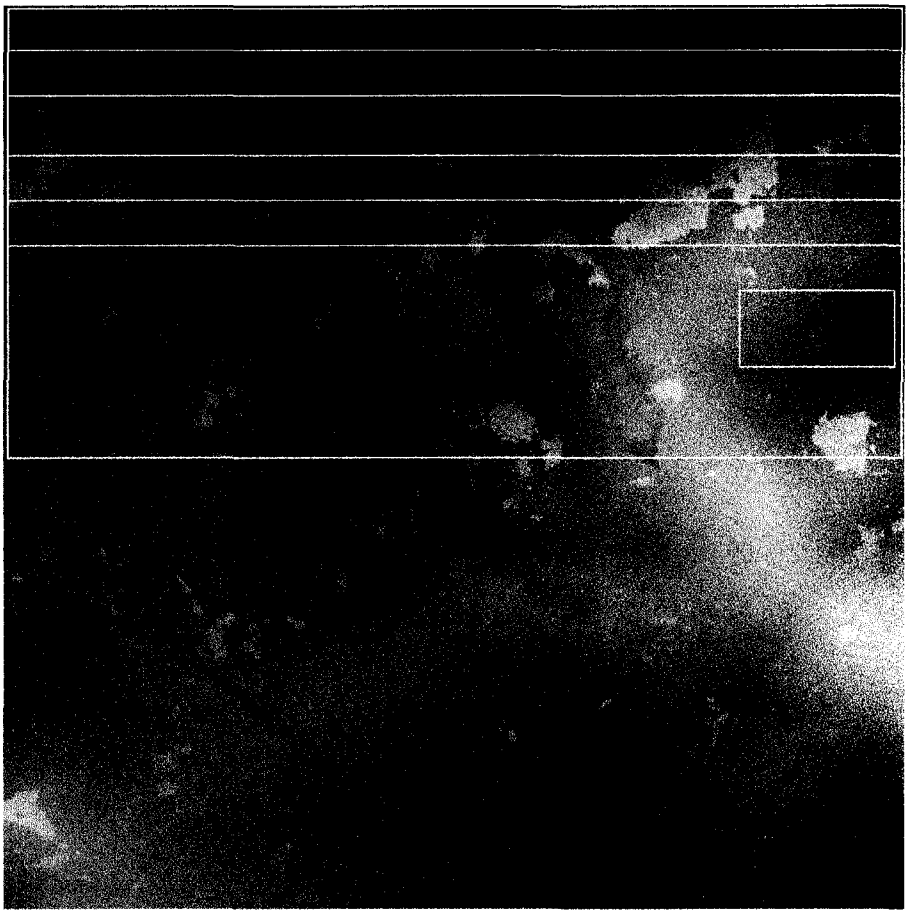

FIG. 3.3. Lower Saxony DEM. The large white rectangle that covers half of the DEM indicates the area studied for the global analysis (3000 transects of 3000 m). The small white rectangle is the treeless section analyzed with spectra, trace moments and structure functions. The white lines represent the 6 individual transects studied with structure functions.

4. METHOD

4.1 Analysis tools

4.1.1 Power spectra

The power spectrum is a tool widely used to verify if a given phenomenon is scaling. It is the modulus squared of the usual Fourier transform, integrated over all angles in Fourier space and ensemble averaged. As mentioned in section 1.1, a certain phenomenon is said to be scaling if it can be represented by power laws in real space. With the help of the tauberian theorem (Feller (1971), Uchaikin and Zolotarev (1999)), it can be shown that power laws in real space give rise to power laws in Fourier space (and vice–versa). So, the (isotropic) power spectrum of a scaling process is given by

$$E(\vec{k}) \sim |\vec{k}|^{-\beta} \tag{4.1}$$

where **k** is the wavenumber and $\beta=1+2H+K(2)$ is the spectral exponent. It can be seen that the monofractal (simple scaling) result is recovered if $K(q)=0$. The power spectrum being a second order moment analysis, it does not give information about the other moments, so this method cannot be used to distinguish between simple and multiscaling.

4.1.2 Trace moments

The trace moments analysis technique is based on equ. (2.8), i.e. on the analysis of the moments of the flux at resolution λ. The procedure is simple and goes as follows. First, the flux ϕ_λ is normalized with the ensemble average $\langle\phi_\lambda\rangle$

of all the samples available. Then spatial averaging is done over sets (lines or squares) of size $l=L/\lambda$, the q^{th} power is taken and the average over all datas available is taken: this gives the moments of the normalized flux for a given value of q. This procedure is done for different values of q, and multiscaling is verified if it follows equ. (2.8). The simple scaling case is when $K(q)=0$, implying that the moments of the normalized flux are equal to 1 for all q.

Contrary to the methods described in sections 4.1.1 and 4.1.3, which work directly on the altitude h, trace moments work on the flux ϕ, which is not directly observable. To obtain ϕ from the height increments, a fractional differentiation of order H or greater must be done (Schertzer and Lovejoy (1987, 1991)): this has the effect of removing the λ^{-H} term in equ. (2.12). A good numerical approximation to this fractional differentiation is to take the modulus of the finite difference gradient (Lavallée et al. (1993)), which corresponds to a differentiation of order H=1 (which is sufficient, because, according to dimensional analysis, H=1/2 in topography).

A technical point here: because of the insufficient dynamical range of the DEMs (see chapter 3), many spurious zero gradients are present in the analyzed transects. Those zero gradients particularly affect the low q statistics, so they are eliminated by doing a fractional integration of order H=0.1 (a filtering in Fourier space with a power law), which is a scale invariant smoothing (the result is a 64 fit field).

4.1.3 Structure functions

The q^{th} order structure function (called the variogram when q=2) is defined as

$$\langle |\Delta h_\lambda|^q \rangle \sim \lambda^{-\xi(q)} \sim l^{\xi(q)} \tag{4.2}$$

where $\xi(q)=qH-K(q)$. It is designed to study the absolute finite difference gradients of the altitude h and is in fact just equ. (2.13). This method could in principle be used to detect multiscaling behaviour because q can be varied (see Lavallée et al. (1993) and Weissel et al. (1994)), but it is not used extensively in this study. In fact it is used only to see more clearly what happens to the scaling when there are trees on the surface and to have a better interpretation of the results (see section 5.3).

4.2 Regions analyzed on each DEM

4.2.1 Continents vs oceans analysis

The comparison between continents and oceans is done via power spectra and trace moments on ETOPO5. Three squares of 5120x5120 km are analyzed in the case of continents and five in the case of oceans (shown on Fig. 3.1). The ensemble average is done over the three (five) squares of continents (oceans) for the two methods of analysis and the results are compared.

4.2.2 Global topography analysis

One dimensional topographic transects are taken from the four DEMs and analyzed with power spectra and trace moments. The transects are chosen so as to maximize the range of scales analyzed. The regions analyzed are shown on Fig. 3.1 (for ETOPO5), 3.2 (for GTOPO30 and the U.S. DEM) and 3.3 (for the Lower Saxony DEM). See table 3.1 for details. In the case of ETOPO5, only transects that are in a narrow strip around the equator are used. This is to have an approximately constant resolution at each latitude. To overcome this problem, the analyses on ETOPO5 could have been done with spherical harmonics, but it would not have been possible to compare with the results of other DEMs.

An important point here: scale invariance is a statistical symmetry (see section 2.2.1). The theory asks that the averages should be on an infinity of independent samples (ensemble average). But all the transects analyzed in this study are correlated because they come from the same region and from the same Earth: in theory, in would take many independent planet Earth and study the same region on each one, something that is of course not possible! So it is important to keep in mind the the averages in this study are only approximations of the required ensemble averages.

4.2.3 Trees analysis

For the power spectra and trace moments analysis methods, two regions of the Lower Saxony DEM are analyzed. The first one is the same as the one in section 4.2.2 and contains trees. The second one is chosen so as to contain no trees and is composed of 500 transects that are 512 m long (shown on Fig. 3.3). The criterion for choosing this particular region is that it must not contain

irregular white patches (that are believed to be trees). For the structure functions analysis, the same 500 treeless transects above and 6 individual transects that are 3 km long (shown in Fig. 3.3) are used. The criterion for choosing the 6 individual transects is that they must contain some irregular white patches.

5. RESULTS AND DISCUSSION

5.1 Continents vs oceans results

A comparison between the spectra from continents and oceans is shown on Fig. 5.1. According to equ. (4.1), a log/log plot of the spectral energy E(k) versus the wavenumber k should give a straight line if the process is scaling. Those spectra are straight over 2 orders of magnitude, implying that they are scaling over that range. There is a break in the scaling at approximately 50 km

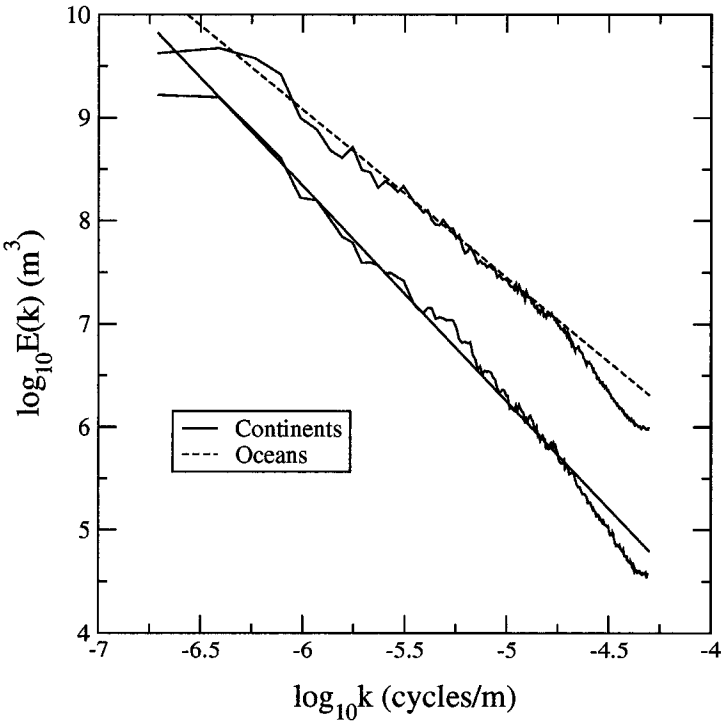

FIG. 5.1. Log/log plot of the spectral energy versus the wavenumber for continents and oceans. The slopes are 2.09 for continents and 1.63 for oceans.

that is probably due to oversampling, because oversampling tends to artificially smooth the datas, which results in a faster spectral fall–off. An important thing to note is that there is a systematic difference in the slope of the spectra: $\beta_{continents}$=2.09 (in agreement with the value $\beta\approx2$ of Vening–Meinesz (1951)) and β_{oceans}=1.63 (in agreement with $\beta\approx1.6–1.8$ of Berkson and Matthews, but less than the values of Bell (1975) ($\beta\approx2$), Fox and Hayes (1985) ($\beta\approx2.5$) and Gibert and Courtillot (1987) ($\beta\approx2.1–2.3$)). The differences between the values of β can probably be explained by the fact that the slope of the spectra depends critically on the amount of data and the range of scales analyzed. In the studies mentioned above, the analyses are on single short transects, meaning that the spectral exponents are not necessarily well estimated and probably explains some of the variability between the results.

The trace moments of the continents and the oceans are shown in Fig.5.2 a,b. According to equ. (2.8), a log/log plot of the normalized moments of the flux (at a certain resolution λ) versus λ should give straight lines if the process is multiscaling. As can be seen on Fig.5.2, the trace moments are straight but seem to have the same problem as the spectra: because of oversampling, the trace moments become flat at large λ. But they are nonetheless an indication that topography is multiscaling (the multiscaling will be showed with more precision in section 5.2).

With the slopes of the trace moments, it is possible to find the K(q) functions for continents and oceans and estimate their universal parameters α and C_1. Figure 5.3 shows the resulting K(q)'s. Equation (2.10) is used to fit those curves, which gives $\alpha_{continents}$=1.77 ($\pm$0.03), $C_{1\ continents}$=0.12 ($\pm$0.001) and α_{oceans}=1.83 ($\pm$0.03), $C_{1\ oceans}$=0.15 ($\pm$0.001). The errors in parenthesis are solely due to the fitting algorithm used and should be taken only as an indication

a)

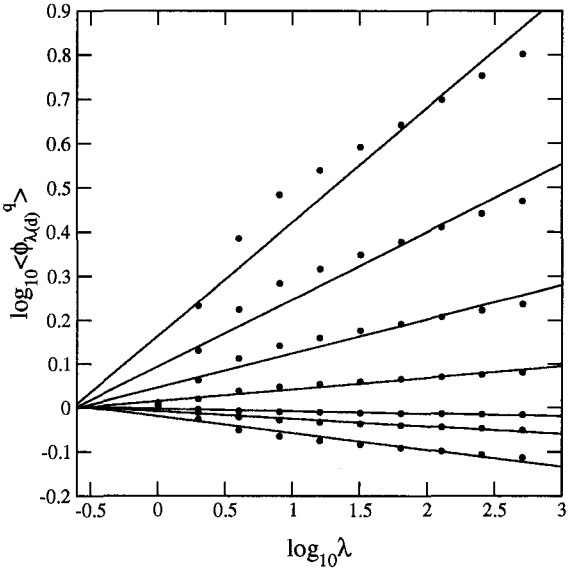

b)

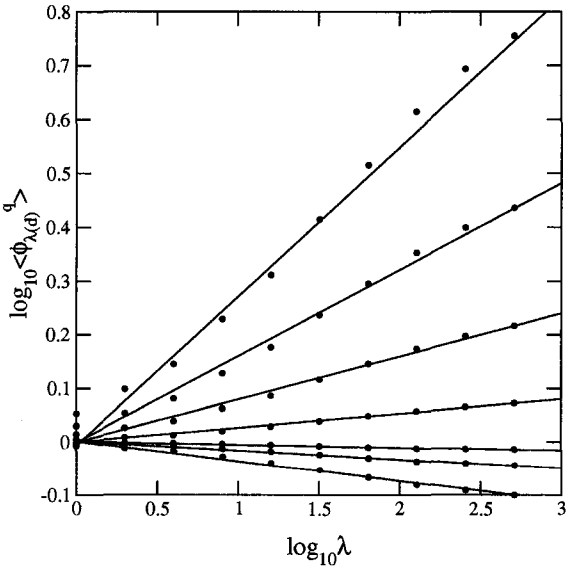

FIG. 5.2. Log/log plot of the normalize trace moments versus the scale ratio λ=L/l for continents and oceans (with L=5120 km). The values of q of each trace moments are, from top to bottom, 2.18, 1.77, 1.44, 1.17, 0.04, 0.12 and 0.51. a) Continents b) Oceans.

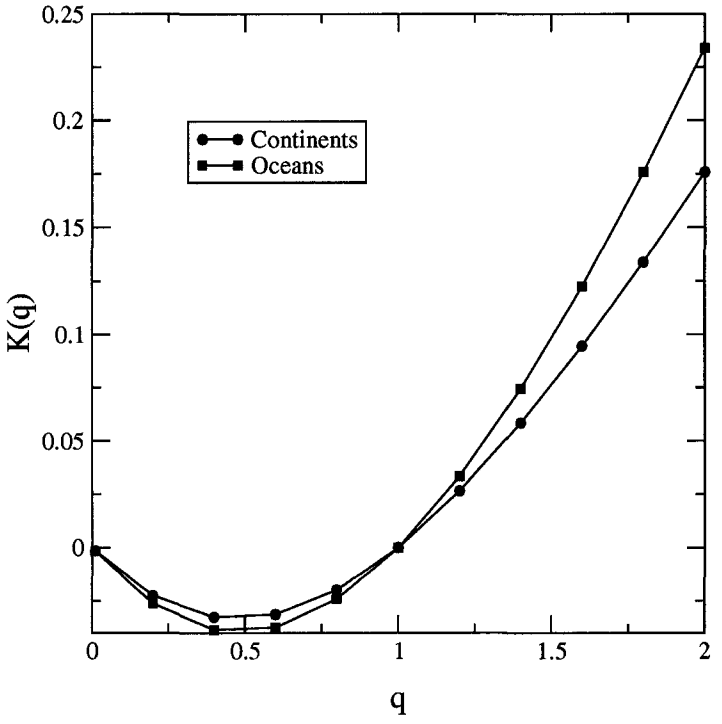

FIG. 5.3. Plot of the moment scaling function K(q) as a function of the moment q (circles correspond to continents and squares to oceans).

(they are only lower bounds). In fact the errors are probably larger than that because each of the point of the K(q) function depends on the slope of the corresponding trace moment: the value of this slope depends on the range of fitting and has also an error due to the fitting algorithm. There is also the error attached to the calculation of the trace moments that must be taken into account, but there are no satisfying error analysis in this formalism yet, so it is difficult to calculate a precise value for the error. With this in mind, it is possible to say that α and C_1 are probably similar for continents and oceans.

With those values of α and C_1, the values of H for continents and oceans can be calculated (see equ. (4.1) and following discussion), which gives $H_c=0.66\pm0.01$ and $H_o=0.46\pm0.01$ (here the errors are due to the fitting algorithm when evaluating β). The H value for oceans is quite near the theoretical value of H=1/2 (see section 1.4), but the H value for continents is systematically larger. So, those results show that the statistics of the flux ϕ are the same for continents and oceans, but the height statistics (see equ. (2.12) and (2.13)) are different because H is different. In fact, a higher value of H for continents means that continental topography is smoother than the sea–floor. It also means that the simple dimensional analysis (with H=1/2) proposed by Lovejoy et al. (1995) for continents does not seem to hold.

There is also another possibility regarding the interpretation of the spectra in Fig. 5.1. The difference in slope between continents and oceans may be due to the fact that the multifractal is conditioned in the case of the continents analysis. If the topography can be thought as a unique multifractal process, then the singularities of continental topography are larger than the ones of the sea–floor (if the reference is the center of the Earth for example). So it means that an analysis on continents is "conditioned" in the sense that the statistics of only the "rare" (large) singularities are taken into account. It is shown in Lovejoy et al. (2000) (in a particular case) that this type of conditioning can lead to a change in the value of β, but this result is hard to obtain and not easily generalizable.

5.2 Global topography results

Figure 5.4 shows the results of the power spectrum analysis over the four DEMs. The log/log plots on Fig. 5.4 gives straight lines over 6 orders of

magnitude, meaning that the scaling is well respected from planetary scales down to a few meters. In fact, at 40 m, there is a little bump that breaks the scaling in the Lower Saxony spectrum, which can probably be explained by the presence of trees on the DEM. See section 5.3 for more details.

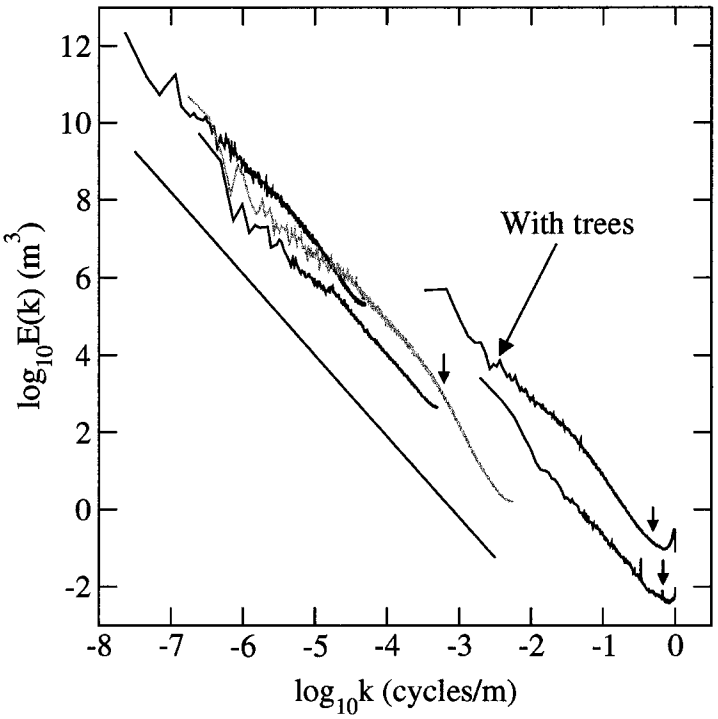

Fig. 5.4. Log/log plot of the spectral energy versus the wavenumber for the four DEMs. From right to left: Lower Saxony (with trees, top), Lower Saxony (without trees, bottom), U.S. (in grey), GTOPO30 and ETOPO5. A reference line of slope –2.10 is on the graph to show the overall slope of the spectra. The little arrows show the frequency at which the spectra are not well estimated, according to equ. (5.1) (for ETOPO5 and GTOPO30, it is well estimated on the whole range).

It is not clear what happens to the scaling of the spectra at high wavenumbers because of the insufficient dynamical range of the transects, which leads to a poor estimate of the spectrum for high wavenumbers. It is possible to find the wavenumber k_{break} at which the spectrum starts to be badly estimated with the following argument. Let $\Delta h_{max}=h_{max}-h_{min}$ be the maximum range of altitude on the data set and Δh_{min} the smallest possible difference on the data set (which is equal to the height of one unit of vertical quantization). The ratio $\Delta h_{max}/\Delta h_{min}$ gives the dynamical range of the data set. Because the spectrum of a scaling process is a decreasing power law, the amplitude of the $k_{min}=1$ sinusoid is proportional to Δh_{max} (or $E(k_{min})\Delta k \approx \Delta h_{max}^2$) and the lowest possible amplitude (which is proportional to Δh_{min}) corresponds to the k_{break} sinusoid (or $E(k_{break})\Delta k \approx \Delta h_{min}^2$), hence

$$\left(\frac{\Delta h_{max}}{\Delta h_{min}}\right)^2 \approx \frac{E(k_{min})}{E(k_{break})} = \left(\frac{k_{min}}{k_{break}}\right)^{-\beta} \Rightarrow k_{break} \approx (h_{max}-h_{min})^{\frac{2}{\beta}} \qquad (5.1)$$

where β is the spectral exponent and $h_{max/min}$ are the maximum/minimum heights on the transects (expressed in digital counts). The wavenumbers at which the spectra start to be badly estimated are shown with arrows on Fig. 5.4 (there are no arrow for ETOPO5 and GTOPO30 because its spectrum is well estimated for all k values). This approximation works particularly well for the U.S. spectrum, where it explains the drop in the high frequencies. In fact, this problem of insufficient dynamical range, which is related to the problem of insufficient statistics and the statistical nature of scale invariance[6], can probably explain

6 If more and more realizations are analyzed, the probability of having higher/lower altitudes increases, so it increases the dynamical range and the chance to observe good scaling over that range.

some scale breaks seen in the litterature that are interpreted as characteristic scales of the process. There is also the problem of oversampling (see section 5.1) that can lead to a fall–off of the spectra at high wavenumber.

Another point worth mentioning is the fact that all the spectra fall "on the same line" (it is important to note that they are all in the same units and are not shifted in the vertical), their range of scaling is at least 3 orders of magnitude each and their ranges overlap. The overlap is important, because it shows that the high wavenumber fall–offs or flattening are artefacts of the particular data set. This result is quite different from that of Sayles and Thomas (1978) who argued that surfaces (natural and man made) exhibit scaling over 8 orders of magnitude. In their case, the range of scaling of their individual data sets was very limited (they used 23 data sets to cover their 8 orders of magnitude) and the shifts in spectral amplitude were more or less arbitrary (Berry and Hannay (1978)). On Fig. 5.4, only the Lower Saxony spectrum does not follow the overall line, but this is probably due to trees (see section 5.3 for details).

The spectra of Fig. 5.4 come from continents (except the one of ETOPO5, which is a continents/oceans mix). To calculate the theoretical spectral exponent predicted by universal multifractals, one must use the H value of the continents ($H_{continents}=0.66$) and the multifractal correction K(2) (calculated with the global values of α and C_1 found with the trace moments (see below)), which gives $\beta=1+2H_c-K(2)=2.10$. A reference line of slope –2.10 is shown on Fig. 5.4 to show that the overall slope is close to –2 (in agreement with Vening Meinesz (1951)), but is also close to the one predicted by universal multifractals.

The trace moments analysis was done on the four DEMs with 7 values of q. Log/log plots of the normalized moments versus λ are shown on Fig. 5.5 a–d. Straight lines are obained on all the DEMs, meaning that equ. (2.8) is obeyed. The slopes of the straight lines are equal to K(q), and the fact that the slopes are different for different values of q implies that $K(q)\neq 0$, so topography is not simple scaling. The point at which all the trace moments converge corresponds to the "effective" outer scale of the cascade. It corresponds to the only non random value, i.e. $\langle \phi_1^q \rangle = 1$ for all q at $l = L_{effective}$, which is where the constant input flux enters the cascade. Concretely, this means that in the study of a particular DEM with a certain limited range of scales, the variability that is observed can be the result of a larger cascade that starts at $L_{effective}$. This effective outer scale can only be estimated by using an infinite ensemble of realizations of the process. But given only one realization (which is the case in this study, because there is only one Earth), $L_{effective}$ corresponds generally to the outer scale of the DEM studied or it can be at smaller. It is interesting to note that the effective outer scale of ETOPO5 is $\approx$20000 km (see Fig. 5.5 a) and not 40000 km (which is the outer scale of the DEM). This means that there is a cascade starting at approximately 20000 km, which is the size of a great circle (the maximum possible size on Earth). In the case of GTOPO30 and the U.S. DEM, the effective outer scale is larger than the DEM outer scale, which is surprising because there is only one realization. This may be due to the fact that the variability is very high (almost half of the region covered in the analyses contains mountains, see Fig. 4.2) or that the fitted lines on Fig. 5.5 b,c are not good because of the flattening of the trace moments at high λ (which can be the result of oversampling, as discussed in section 5.5).

a)

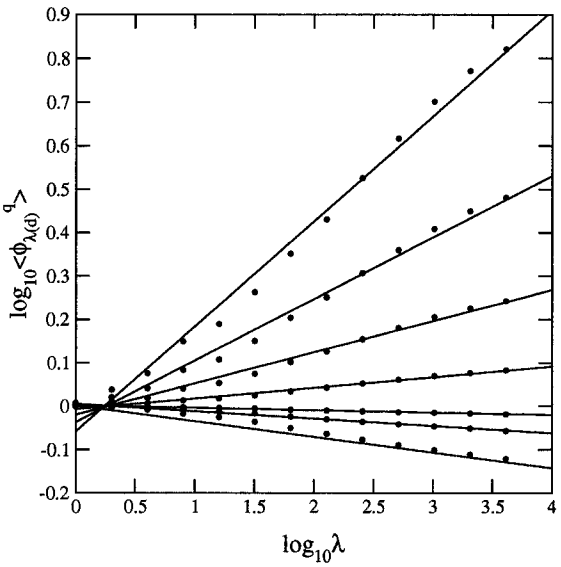

b)

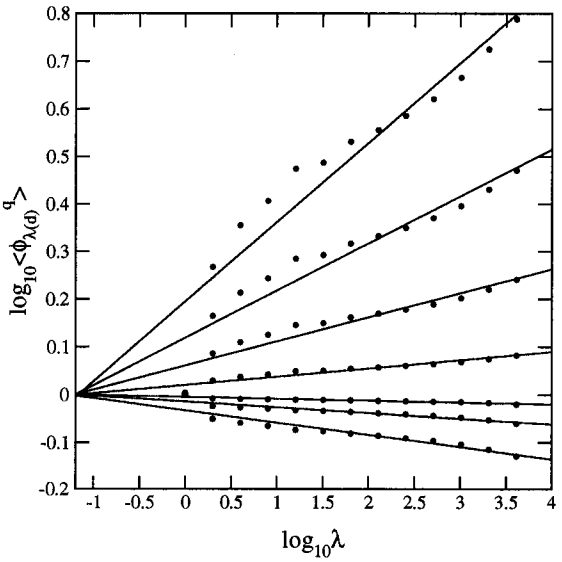

Fig. 5.5. Log/log plot of the normalize trace moments versus the scale ratio $\lambda=L_{DEM}/l$ for each DEMs. The values of q of each trace moments are, from top to bottom, 2.18, 1.77, 1.44, 1.17, 0.04, 0.12 and 0.51. a) ETOPO5, L_{ETOPO5}=40000 km b) GTOPO30, $L_{GTOPO30}$=4096 km.

c)

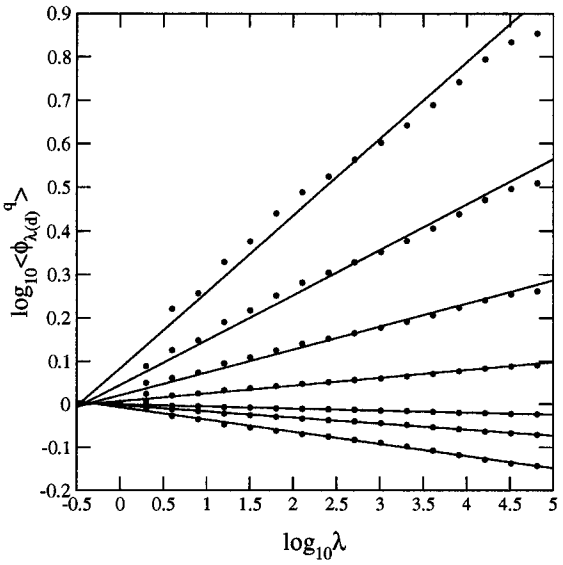

Fig. 5.5. Log/log plot of the normalized trace moments versus the scale ratio λ for each DEMs (continued). c) U.S. DEM, L_{US}=5898 km d) Lower Saxony DEM, $L_{Lower\ Saxony}$=3000 m.

To see more clearly the exact form of K(q), plots of the slopes of the trace moments for each DEM as a function of q are shown on Fig. 5.6 and 5.7. Those curves are nonlinear, showing that topography is not simple scaling but multiscaling. Another interesting point is the linear behaviour of the K(q) curves. This linear behaviour is the signature of a second order multifractal phase transition (Schertzer and Lovejoy (1992)). This phase transition is caused by the fact that, on a given realization, there is an maximum singularity γ_s (larger singularities are almost surely not present on the realization). This implies that for $q>q_s$, K(q) becomes linear:

$$K(q)=\gamma_s(q-q_s)+K(q_s) \qquad for\, q>q_s \tag{5.2}$$

The estimated values of q_s (obtained from Fig. 5.6 by measuring at which q the function K(q) becomes linear) are approximately 3.5 for all the data sets. This means that, for $q>q_s$, the function K(q) becomes less interesting, because the slope is given by γ_s, which is a random variable that depends on the realization of the process.

The K(q) curves of Fig. 5.6 and 5.7 are fitted with equ. (2.10) in the range $0\leq q\leq 1$ (to be sure to avoid any pollution from the linear behaviour). The values obtained for the parameters can be seen in Table 5.1. These results can be compared to other studies on topography (see Table 5.1). Even if those analyses are on different parts of the world and are on different ranges of scales, the parameters obtained are not too different from the ones of this study. Of course, it is important to consider that α and C_1 are statistical in nature, and that there are a lot less statistics (in terms of number of pixels studied) in the previous studies then in the present one, so it is normal that there is some variability between them.

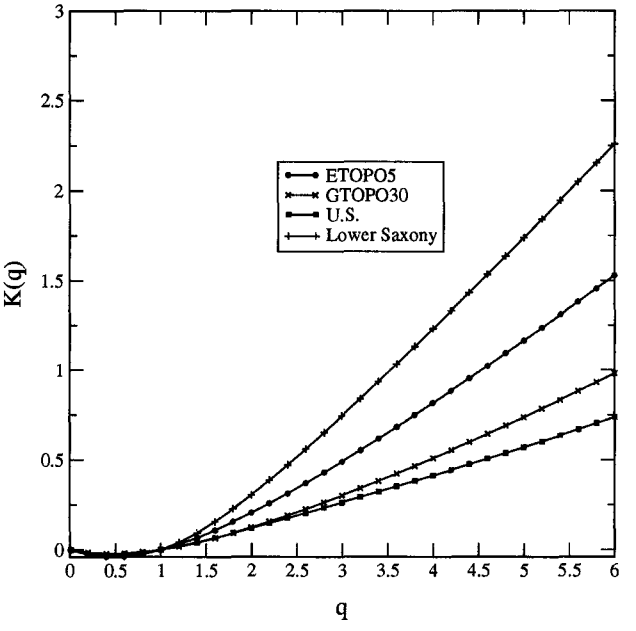

Fig. 5.6. Plot of the moment scaling function K(q) as a function of the moment q for the four DEMs (+ correspond to Lower Saxony, squares to U.S., X to GTOPO30 and circles to ETOPO5).

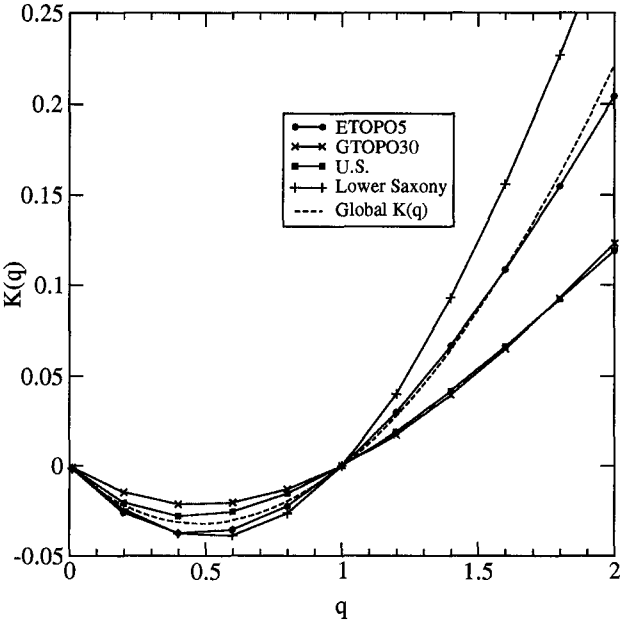

FIG. 5.7. Zoom of Fig.5.6. The dotted line corresponds to the "mean" K(q) with parameters α=1.79 and C_1=0.12.

Data sets	*Horizontal resolution*	*Regions analyzed (in pixels)*	α	C_1	*References*
ETOPO5	≈10 km	500x4000	1.72	0.14	---
GTOPO30	≈1 km	1225x4096	1.77	0.08	---
U.S.	90 m	2500x65536	1.51	0.09	---
Lower Saxony	50 cm	3000x6000	2.00	0.17	---
Deadman's Butte	50 m	512x512	1.9	0.045	Lavallée et al. (1993)
French topography	1 km	512x512	1.7	0.075	Lavallée et al. (1993)
U.S.	90 m	20 x 512x512	1.70	0.07	Pecknold et al. (1997)

TABLE 5.1. Universal parameters obtained for the four datasets analyzed. Also shown are the parameters obtained in other studies.

The similarity between the α and C_1 parameters between all these studies suggests the introduction of a "global" K(q) function that would describe the statistics of the Earth's topography at all scales. Even if the trace moments are on continents and oceans (in the case of ETOPO5), it is reasonable to make the hypothesis that continents and oceans are described by the same K(q), because the statistics of their fluxes ϕ are similar (i.e. they have the same α and C_1 parameters, see section 5.1). An approximation of this global K(q) would be to take the average of the parameters obtained in this study (α=1.79±0.18 and C_1=0.12±0.04, where the uncertainties are equal to one standard deviation) and plot the corresponding K(q) (dotted line on Fig. 5.7). One way to test if the

hypothesis of the global K(q) is plausible is by checking if there is a cascade going "uninterrupted" from planetary scales down to a certain smaller scale. This can be done with the help of the trace moments of the four DEMs (Fig. 5.5 a–d) and the global K(q). The goal of this test is to show that all the trace moments of the four DEMs can be though as a single trace moment representing the cascade at all scales. Concretely this means that, if there is indeed a global cascade, then the trace moments of the four DEMs could be shifted appropriately (with the global K(q) as the only "tuning device") so that they all "align themselves" for a specific value of q, and should do so for all the different values of q. Those shifts represent the missing variability due to the fact that there is only one realization of the Earth, so it is necessary to statistically take it into account.

So the question here is "What are the horizontal and vertical shifts and how can they be calculated?" For the horizontal shifts, the first thing to consider is the outer scale L_{outer} of the process. If the process is a cascade, then the scale at which the cascade starts may be as large as the size of a great circle, which is approximately 20000 km. This is justified because the effective outer scale on Fig. 5.5 a (i.e. the converging point of all the trace moments) is approximately 20000 km. By fixing this outer scale, it is possible to calculate all the $\lambda=L_{outer}/l$ of the DEMs (this corresponds to a shift on the horizontal axis). To justify the vertical shifts, one must use the factorization property of cascades. If $<\phi_{\lambda 1}{}^{q}>$ is the result of large scale variability from planetary scales to a scale l_1 that is λ_1 times smaller (equal to the data set largest scale, $l_1=L_{DEM}=L_{outer}/\lambda_1$) and l_2 is the scale we are stuying on the data set (e.g. $l_2=L_{DEM}/\lambda_2$), then factorization implies

$$\langle \phi^q_{\lambda_1\lambda_2} \rangle = \langle \phi^q_{\lambda_1} \rangle \langle \phi^q_{\lambda_2} \rangle = \lambda_1^{K(q)} \langle \phi^q_{\lambda_2} \rangle \qquad (5.2)$$

where $<\phi_{\lambda 2}^q>$ is the variability calculated from the DEM only (which is limited because there is only one single realization) and $<\phi_{\lambda 1 \lambda 2}^q>$ is the "true" variability that takes into account the variability coming from the larger scales. On a log/log plot, the multiplicative factor $<\phi_{\lambda 1}^q>$ (i.e. the variability due to the larger scales) of equ. (5.2) becomes a linear shift in the trace moments, corresponding to a linear vertical shift on Fig.5.5 a–d[7]. So the shifts $S=\log_{10}<\phi_{\lambda 1}^q>$ can be estimated with

$$S = K(q)\log_{10}\left(\frac{L_{outer}}{L_{DEM}}\right) \tag{5.3}$$

where K(q) is the global moment scaling function, L_{outer}=20000 km and $L_{DEM}=L_{ETOPO5}$, $L_{GTOPO30}$, L_{US} and $L_{Lower\ Saxony}$ are the outer scales of each DEM. Figure 5.8 shows the trace moments of three DEMs[8] shifted according to equ. (5.3). The vertical shifts are quite accurate if we take into account the fact they depend only on one global K(q) (which itself depends on only two parameters). This is an indication that the hypothesis of the global K(q) may be justified. The lines obtained are not exactly straight, but are more like a small oscillation around a straight line (this is more apparent for large values of q). Those oscillations are probably due to anisotropies. In fact, the trace moment analysis is defined isotropically in this study, i.e. the resolution λ is defined isotropically by coarse graining over squares at all scales. For "weak" anisotropies, this method is insensible (most of the anisotropies are washed out), but when they are "stronger", their effect can be seen. It can be shown (Lovejoy, S. (2001),

7 This factor represents the variability of the samples analyzed. If, for example, all the 3 km x 3 km sections of the world (with a resolution of 50 cm) would have been analyzed, then the variability would have been higher, so the vertical shift would have been larger and the converging point would have been at a lower value of λ.

8 The trace moments of GTOPO30 are not on Fig. 5.8 because its scaling range is already contained in the U.S. range, so it is unnecessary to overcrowd the graph.

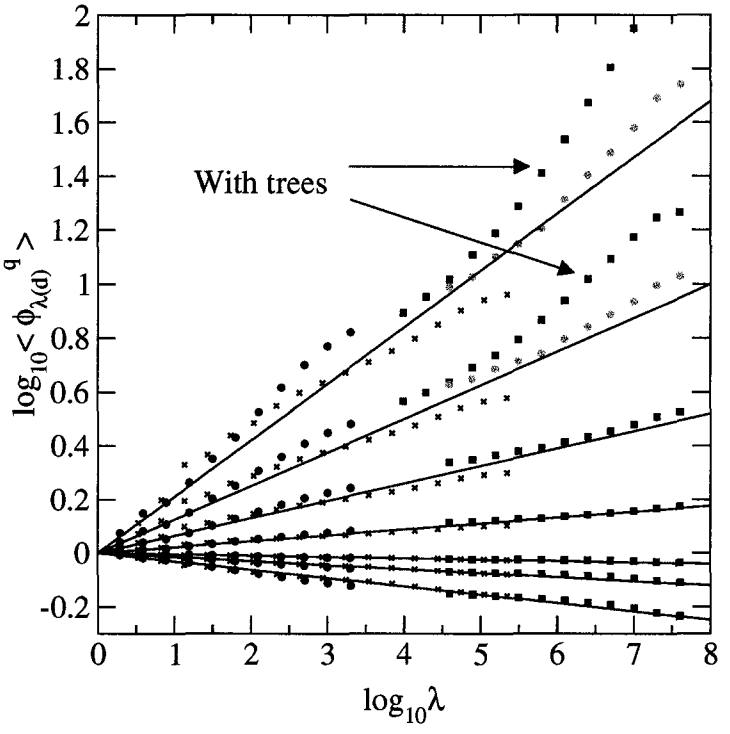

FIG. 5.8. Log/log plot of the normalized trace moments versus the scale ratio $\lambda=L_{outer}/l$ (with L_{outer}=20000 km) for the three DEMs (circles correspond to ETOPO5, X to U.S. and circles to Lower Saxony). The solid lines are there to distinguish between each value of q (from top to bottom, q=2.18, 1.77, 1.44, 1.17, 0.04, 0.12 and 0.51). The trace moments of the Lower Saxony DEM with trees for q=1.77 and q=2.18 are on the graph (indicated by arrows).

personal communication) that on a multifractal simulation that is rotation dominant (i.e. the scaling is anisotropic and "rotates" as the scale is changed) that the trace moments are oscillating around a straight line. This means that, as a first approximation, isotropic methods are justified but a complete analysis of anisotropies (that are generated by the different geomorphological processes like crust generation and erosion) would require the use of Generalized Scale Invariance (Schertzer and Lovejoy (1987, 1991)). So, by taking that into account, it is possible to say that the trace moments obtained on Fig. 5.8 are oscillating

around a straight line over 6 orders of magnitude (there is a break at ≈40 m that is discussed in section 5.3), meaning that the Earth's topography is multiscaling over that range.

5.3 Trees results

When a DEM (like the Lower Saxony DEM) has a very high resolution, small structures are resolved. Those structures can be natural (like trees) or man made (like buildings, highways). Indeed, those structures pose non trivial problems. For example, in the case of stereophotography, their measurement is uncertain (it depends on what are the angles between the cameras, and how the algorithm deals with this problem). Also, if one wants to remove ("smooth") them from the DEM, what are the hypothesis that must be used. Those are important points that must be investigated before going further in the analysis of multiscaling in the presence of structures like trees. The irregular white patches that can be seen on Fig. 4.3 are believed to be trees.

A comparison between the spectra of a "normal" region (containing trees) and a treeless region of the Lower Saxony DEM is on Fig. 5.4. There is a little bump at approximately 40 m in the top spectrum that is not present in the lower one, meaning that the trees are probably causing this bump. Also, the top spectrum does not follow the "overall" spectrum (it is shifted vertically with respect to the others), which is not the case with the treeless spectrum. This can be explained by the fact that trees are not a part of natural topography, they are an addition to the relief, so they add spectral energy to the spectrum, which results in a vertical shift. With this new treeless spectrum, one could also be tempted to say that the scaling is respected down to 1 m, but this result should not be taken too literally: it could be an artefact of the particular area chosen for

the analysis. In fact, it is shown with structure functions (see below) that the treeless region is too smooth, it is almost not a fractal at all.

The same two regions are analyzed with trace moments. Figure 5.9 (see also Fig. 5.8) shows the comparison between the trace moments of the "normal" and the treeless regions (the vertical shifts are calculated in the same manner as in section 5.2). It is clear from this graph that multiscaling is broken at around 40 m (dotted line). For low q values, the break is less apparent, but for larger q values, the break is evident. This means that, for "small" singularities, the

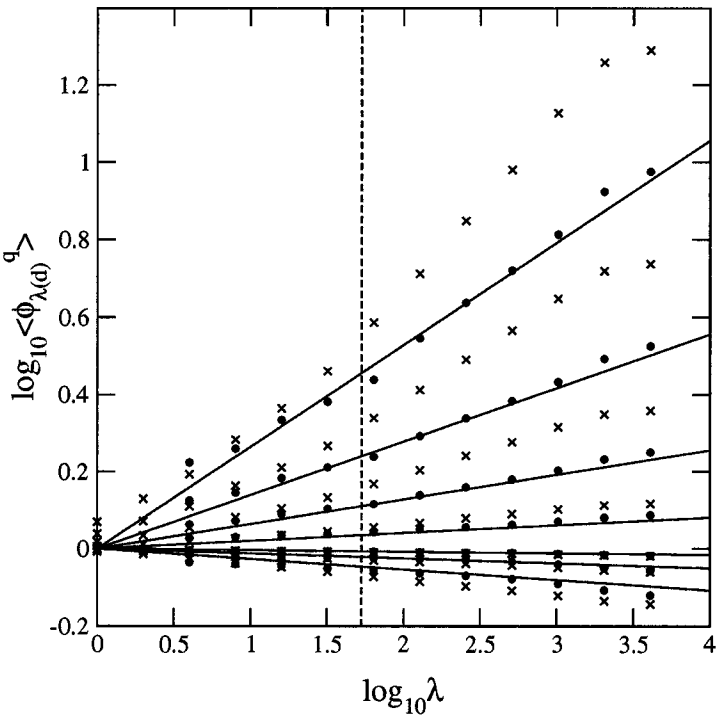

FIG. 5.9. Log/log plot of the normalize trace moments versus the scale ratio λ=L/l for the Lower Saxony DEM (L=3 km). Circles correspond to the treeless part and X to the part containing trees. The values of q of each trace moments are, from top to bottom, 2.18, 1.77, 1.44, 1.17, 0.04, 0.12 and 0.51.

multiscaling is not so bad, but for "large" singularities (like trees), something is spoiling the statistics. This scale break disappears in the treeless trace moments, an indication that the trees can affect the scaling in some way, but it is not really clear if this difference is really due to the trees or only an artefact of the particular area chosen for the analysis (same situation as for the spectrum).

To see if the treeless region is "pathological", the structure function (with q=1) of the region is taken and the results are shown on Fig. 5.10. A reference line of slope 1 is also on the graph. The structure function is not too far from the reference line, meaning that $\xi(1)=H+K(1)\approx 1$, implying that $H\approx 1$. This is a limit

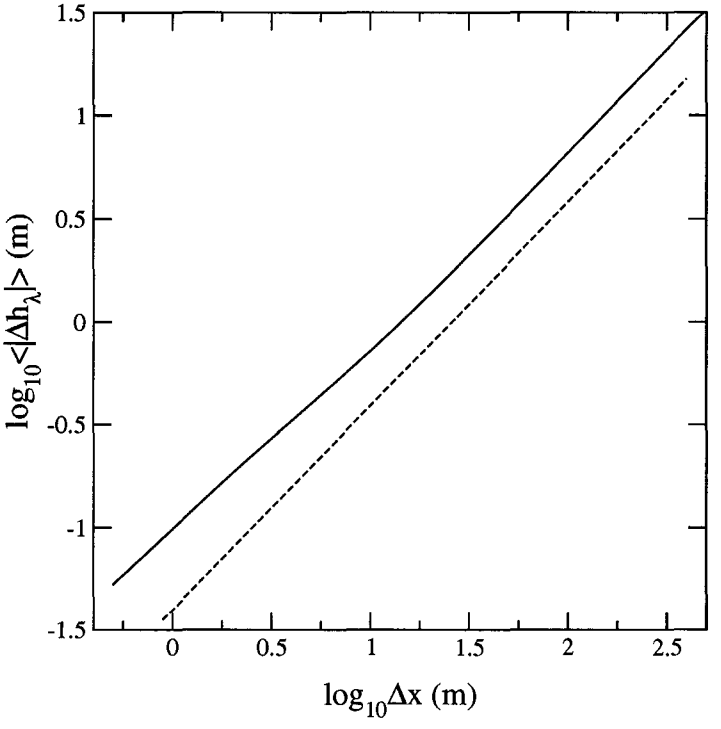

FIG. 5.10. Log/log plot of the height increments versus horizontal increments for the treeless part of the Lower Saxony DEM. The dotted line has a slope of 1.

case because $<|\Delta h|>\sim\Delta x$, which means that the surface may not be a fractal at all, it is really smooth compared to the rest of the DEM. So the spectrum and trace moments results obtained on the treeless region should not be taken as an clear demonstration that the multiscaling goes down to the smallest scale available (i.e. 0.5 m), because the treeless region is very smooth and may not be a fractal (perhaps the region was cleared and landscaped).

The structure functions (with q=2) of the 6 individual transects of the Lower Saxony DEM indicated on Fig. 4.3 (those transects include trees) are shown on Fig. 5.11. There seems to be a break in the structure functions at varying horizontal increments Δx (between approximately 30 m and 160 m), depending on the transect studied. This suggest that it is not the characteristic length in the horizontal that is fundamental. A closer look at Fig. 5.11 shows that the breaks in the scaling seem to occur when $<|\Delta h|>\approx 9$ m (dotted line on Fig. 5.11). Of course this is not absolutely clear cut, but the two "regimes" seem to be separated by a characteristic length in the vertical. This makes sense when one looks at a typical transect of Lower Saxony (Fig. 5.12). The spikes on this transect have a height of about 10 m (except the large one on the right), which can be the typical height of a tree and is quite close to the vertical characteristic length found with the structure functions.

It is this characteristic length $\Delta h\approx 9$ in the vertical that imposes a characteristic length $\Delta x\approx 40$ in the horizontal and breaks the scaling in the spectrum and the trace moments analyses. This can be readily understood with the following argument. From Fig. 5.11, it is possible to find $\xi(2)=2H-K(2)\approx 0.9$ (for $<|\Delta h|>>9$), which gives $H\approx 0.55$ for the Lower Saxony DEM. With this value of H, one finds that $<|\Delta h_{break}|>\approx (\Delta x_{break})^H \approx 40^H = 7.6$ m, which is approximately the typical height of a tree. This means that one must study

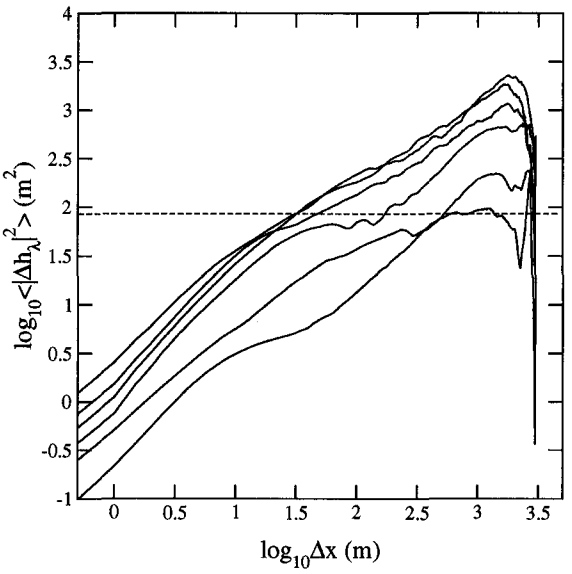

FIG. 5.11. Log/log plot of the variance of the height increments versus horizontal increments for the 6 individual transects of the Lower Saxony DEM. The horizontal dotted line shows the vertical characteristic length that imposes a horizontal break in the scaling.

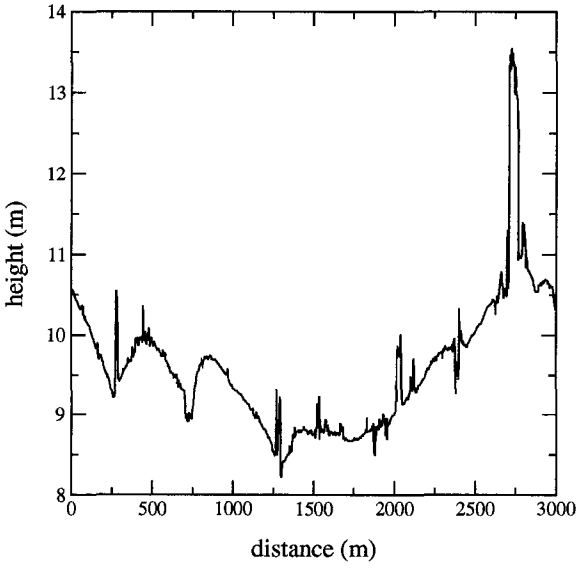

FIG. 5.12. Typical transect of the Lower Saxony DEM.

horizontal increments Δx that are large enough (in this case, $\Delta x > 40$ m) so that the height of the terrain (around the tree) his larger than the typical height of a tree, which has the effect of drowning the statistics of the trees in those of topography.

All this leads to the conclusion that the presence of trees on the Lower Saxony DEM explains the break in the multiscaling. This is in contradiction with Dietler and Zhang (1992) who argue, without any supporting analysis, that the statistics of all sorts of natural and man–made structures (like trees, buildings, highways, etc) are probably negligible. According to the above results, this is not the case. These results can have important consequences for future studies on multiscaling. In the cases where there are no such structures, then the results can be an artefact of the particular area chosen for the analysis (e.g. it is too smooth, because it is a region cleared or landscaped by humans). It can also mean that, because a large part of the continents are covered with small structures, the multiscaling at very small scales is masked by the statistics of those structures and will be difficult to probe.

6. CONCLUSION

Because of the great spatial variability of topography over wide ranges of scales, scaling is an indispensable tool for tackling the problem compared to the conventional models that operate over a limited range of scales. By analyzing 4 large datasets over a wide range of scales, this study shows that the fluxes of continents and oceans have the same statistical properties (i.e. the same universal parameters α and C_1) but are different in their height statistics ($H_{continents}$=0.66 and H_{oceans}=0.46). It also shows that the Earth's topography is multiscaling from planetary scales down to (at least) 40 m. This multiscaling implies that fractal geometry can at best be an acceptable approximation around the mean (Fig. 5.6 and 5.7 show that the K(q) curves are nearly flat at q=1), but becomes less and less precise for the extremes. In other words, topography is not fractal but multifractal.

The trace moments of Fig. 5.8 show that topography can be the result of a cascade going from 20000 km to (at least) 40 m. This can be infered by the fact that, to within a good approximation, all the statistics for weak and strong gradients (low and high q's) over this scale range can be well represented by a unique K(q) function. This last assumption is supported by the fact that the fluxes of continents and oceans have the same statistical properties. The universal multifractal parametrization (equ. (2.10)) seems to represent well the form of this global K(q) function with α=1.79 and C_1=0.12. Together with H, those three fundamental parameters gives a statistical characterization of topography over (at least) 6 orders of magnitude.

The break in the multiscaling at approximately 40 m is probably due to trees. This can be explained by the fact that they indroduce a characteristic length in the vertical that is approximately the height of a normal tree ($\approx$9 m) which imposes a scale break in the horizontal at approximately 40 m.

It is important to point out that the analyses of topography in this study are isotropic, meaning that anisotropies are largely washed out. But, at a certain statistical level, all types of relief are more or less the same: it is the different geomorphological processes (like crust generation and erosion) that generate the anisotropy. This anisotropy can be quantified with the help of Generalized Scale Invariance (Schertzer and Lovejoy (1987, 1991)). So the method outlined in this study, combined with Generalized Scale Invariance to take into account anisotropy, opens promising new avenues toward a complete statistical description of topography, and maybe surfaces elsewhere (where Schmittbuhl et al. (1995), for example, has found evidences of multifractality in laboratory crack surfaces).

BIBLIOGRAPHY

Aviles, C. A., Scholz, C. H. and Boatwright, J. (1987). Fractal analysis applied to characteristic segments of the San Andreas fault. *J. Geophys. Res.*, 92, B1, pp. 331–344.

Balmino, G., Lambeck, K. and Kaula, W. (1973). A spherical harmonic analysis of the Earth's topography. *J. Geophys. Res.*, 78, 2, pp. 478–481.

Barenblatt, G. I., Zhivago, A. V., Neprochnov, Y. P. and Ostrovskiy, A. A. (1984). The fractal dimension: a quantitative characteristic of ocean–bottom relief. *Oceanology*, 24, 6, pp. 695–697.

Bell, T. H. (1975). Statistical features of sea–floor topography. *Deep–Sea Research*, 22, pp. 883–892.

Berkson, J. M., and Matthews, J. E. Statistical properties of sea–floor roughness, in *Acoustics and the Sea–Bed*, edited by Pace, N. G. (Bath University Press, Bath).

Berry, M. V. and Hannay, J. H. (1978). Topography of random surfaces. *Nature*, 273, p. 573.

Burrough, P. A. (1981). Fractal dimensions of landscapes and other environmental data. *Nature*, 294, pp. 240–242.

Dodds, P. S. and Rothman D. H. (2000). Scaling, universality, and geomorphology. *Annu. Rev. Earth Planet. Sci.*, 28, pp. 571–610.

Dietler, G. and Zhang, Y. (1992). Fractal aspects of the Swiss landscape. *Physica A*, 191, pp. 213–219.

Falconer, K. *Fractal geometry: Mathematical foundations and applications* (John Wiley and sons, Chichester, 1990).

Feller, W. *An Introduction to Probability Theory and its Applications, vol. 2* (John Wiley and sons, New York, 1971).

Fox, C. G. and Hayes, D. E. (1985). Quantitative methods for analyzing the roughness of the seafloor. *Rev. Geophys.*, 23, pp. 1–48.

Gallant, J. C., Moore, I. D., Hutchinson, M. F. and Gessler, P. (1994). Estimating fractal dimension of profiles: a comparison of methods. *Mathematical Geology*, 26, 4, pp. 455–481.

Gibert, D. and Courtillot, V. (1987). Seasat altimetry and the South Atlantic geoid 1. Spectral analysis. *J. Geophys. Res.*, 92, B7, pp. 6235–6248.

Gilbert, L. E. (1989). Are topographic data sets fractal? *PAGEOPH*, 131, pp. 241–254.

Goodchild, M. F. (1980). Fractals and the accuracy of geographical measures. *Mathematical Geology*, 12, 2, pp. 85–98.

Grassberger, P. (1983). Generalized dimensions of strange attractors. *Phys. Rev. Lett.*, A97, 6, pp. 227–230.

Halsey, T. C., Jensen, M. H., Kadanoff, L. P., Procaccia, I. and Shraiman, B. (1986). Fractal measures and their singularities: the characterization of strange sets. *Phys. Rev. A*, 33, 2, pp. 1141–1150.

Heiskanen, W. A. and Vening Meinesz, F. A. *The Earth and its gravity field* (McGraw–Hill, New–York, 1958).

Hentschel, H. G. E. and Procaccia, I. (1983). The infinite number of generalized dimensions of fractals and strange attractors. *Physica D*, 8, pp. 435–444.

Herzfeld, U. C., Kim, I. I. and Orcutt, J. A. (1995). Is the ocean floor a fractal? *Mathematical Geology*, 27, 3, pp. 421–462.

Herzfeld, U. C. and Overbeck, C. (1999). Analysis and simulation of scale–dependent fractal surfaces with application to seafloor morphology. *Computers & Geosciences*, 25, pp. 979–1007.

Huang, J. and Turcotte, D. L. (1989). Fractal mapping of digitized images: application to the t opography of Arizona and comparisons with synthetic images. *J. Geophys. Res.*, 94, B6, pp. 7491–7495.

Huang, J. and Turcotte, D. L. (1990). Fractal image analysis: application to the topography of Oregon and synthetic images. *J. Opt. Soc. Am. A*, 7, 6, pp. 1124–1130.

Klinkenberg, B. and Goodchild, M. F. (1992). The fractal properties of topography: a comparison of methods. *Earth surface processes and landforms*, 17, pp. 217–234.

Lambeck, K. *Geophysical geodesy: the slow deformations of the Earth* (Oxford University Press, New York, 1988).

Lavallée, D., Lovejoy, S., Schertzer, D. and Ladoy, P. Nonlinear variability of landscape topography: multifractal analysis and simulation, in *Fractals in Geography*, edited by De Cola, L. and Lam, N. (Prentice–Hall, New Jersey, 1993).

Lovejoy, S., Lavallée, D., Schertzer, D. and Ladoy, P. (1995). The $l^{1/2}$ law and multifractal topography: theory and analysis. *Nonlinear Processes in Geophysics*, 2, pp. 16–22.

Lovejoy, S. and Schertzer, D. (1990). Our multifractal atmosphere: A unique laboratory for non–linear dynamics. *Physics in Canada*, 46, 4.

Lovejoy, S. and Schertzer, D. Multifractal analysis techniques and the rain and cloud fields from 10^{-3} to 10^{6} m, in *Non–linear Variability in Geophysics*, edited by Schertzer, D. and Lovejoy. S. (Kluwer Academic Publishers, Netherlands, 1991).

Lovejoy, S., Schertzer, D. and Stanway, J. D. (2001). Direct evidence of atmospheric cascades from planetary scales down to 1 km. *Physical Review Letters*, 86, p. 5200.

Lovejoy, S., Schertzer, D., Tessier, Y. and Gaonac'h, H. (2001). Multifractals and resolution–independent remote sensing algorithms: the example of ocean color. *Int. J. Remote Sensing*, 22, p. 1191.

Mandelbrot, B. B. (1967). How long is the Coast of Britain? Statistical self–similarity and fractional dimension. *Science*, 156, pp. 636–638.

Mandelbrot, B. B. (1975). Stochastic models for the Earth's relief, the shape and the fractal dimension of the coastlines, and the number–area rule for islands. *Proc. Nat. Acad. Sci. USA*, 72, 10, pp. 3825–3828.

Mareschal, J.–C. (1989). Fractal reconstruction of sea–floor topography. *PAGEOPH*, 131, pp. 197–210.

Mark, D. M. and Aronson, P. B. (1984). Scale–dependent fractal dimensions of topographic surfaces: an empirical investigation, with applications in geomorphology and computer mapping. *Mathematical Geology*, 16, 7, pp. 671–683.

McKenzie, D. P. (1967). Some remarks on heat flow and gravity anomalies. *J. Geophys. Res.*, 72, 24, pp. 6261–6273.

Meneveau, C. and Streenivasan, K. R. (1987). Simple multifractal cascade model for fully developed turbulence. *Phys. Rev. Lett.*, 59, 13, pp. 1424–1427.

Monin, A. S. and Yaglom, A. M. *Statistical Fluid Mechanics: Mechanics of Turbulence, vol. 2* (MIT Press, Cambridge, 1975).

Okubo, P. G. and Aki, K. (1987). Fractal geometry in the San Andreas fault system. *J. Geophys. Res.*, 92, B1, pp. 345–355.

Parisi, G. and Frisch, U. On the singularity structure of fully developed turbulence, in *Turbulence and Predictability in Geophysical Fluid Dynamics and Climate Dynamics*, edited by Ghil, M., Benzi, R. and Parisi., G. (North Holland, Amsterdam, 1985).

Parker, R. L. and Oldenburg, D. W. (1973). Thermal model of ocean ridges. *Nature Physical Science*, 242, pp. 137–139.

Parsons, B. and Sclater, J. G. (1977). An analysis of the variation of ocean floor bathymetry and heat flow with age. *J. Geophys. Res.*, 82, 5, pp. 803–827.

Pecknold, S., Lovejoy, S., Schertzer, D. and Hooge, C. Multifractal and resolution dependence of remotely sensed data: GSI and GIS, in *Scale in Remote Sensing and GIS*, edited by Quattrochi, D. A. and Goodchild, M. F. (CRC Press, 1997).

Prey, A. (1922). Darstellung der Höhen– und Tiefenverhältnisse der Erde durch eine Entwicklung nach Kugelfunktionen bis zur 16. Ordnung. *Abhandl. Ges. Wiss. Göttingen, Math.–physik. Kl.*, N.F., 11, 1.

Richardson, L. F. (1961). The problem of contiguity: an appendix to statistics of deadly quarrels. *Gen. Syst. Yearb.*, 6, pp. 139–187.

Smorodnitsky, G. and Taqqu, M. S. *Stable Non–Gaussian Random Processes* (Chapman & Hall, New York, 1994).

Sayles, R. S. and Thomas, T. R. (1978). Surface topography as a nonstationary random process. *Nature*, 271, pp. 431–434.

Schertzer, D. and Lovejoy, S. (1983). On the dimension of atmospheric motions. *Proceedings, 4th Symp. of Turbulent Shear Flows*, 11.1–11.8.

Schertzer, D. and Lovejoy, S. (1987). Physical modeling and analysis of rain and clouds by anisotropic scaling multiplicative processes. *J. Geophys. Res.*, 92, D8, pp. 9693–9714.

Schertzer, D. and Lovejoy, S. Nonlinear geodynamical variability: multiple singularities, universality and observables, in *Non–linear Variability in Geophysics*, edited by Schertzer, D. and Lovejoy. S. (Kluwer Academic Publishers, Netherlands, 1991).

Schertzer, D. and Lovejoy, S. (1992). Hard and soft multifractal processes. *Physica A*, 185, pp. 187–194.

Schertzer, D. and Lovejoy, S. (1997). Universal multifractals do exist! *Journal of Applied Meteorology*, 36, pp. 1296–1303.

Schmittbuhl, J., Schmitt, F. and Scholz, C. (1995). Scaling invariance in crack surfaces. *J. Geophys. Res.*, 100, B4, pp. 5953–5973.

Sclater, J. G., Anderson, R. N. and Lee Bell, M. (1971). Elevation of ridges and evolution of the Central Eastern Pacific. *J. Geophys. Res.*, 76, 32, pp. 7888–7915.

Strogatz, S. H. *Nonlinear Dynamics and Chaos* (Addison–Wesley, Reading, 1994).

Tchiguirinskaia, I., Lu, S., Molz, F. J., Williams, T. M. and Lavallée, D. (2000). Multifractal versus monofractal analysis of wetland topography. *Stochastic Environmental Research and Risk Assessment*, 14, pp. 8–32.

Turcotte, D. L. (1989). Fractals in geology and geophysics. *PAGEOPH*, 131, pp. 171–196.

Turcotte, D. L. Fractals and chaos in geology and geophysics (Cambridge University Press, Cambridge, 1992).

Turcotte, D. L. and Oxburgh, E. R. (1967). Finite amplitude convective cells and continental drift. *J. Fluid Mech.*, 28, part 1, pp. 29–42.

Uchaikin, V. V. and Zolotarev, V. M. *Chance and Stability: Stable distributions and their applications* (VSP, Utrecht, 1999).

Veneziano, D. and Iacobellis, V. (1999). Self–similarity and multifractality of topographic surfaces at basin and subbasin scales. *J. Geophys. Res.*, 104, B6, pp. 12797–12812.

Vening Meinesz, F. A. (1951). A remarkable feature of the Earth's topography, origin of continents and oceans. *Proc. Koninkl. Ned. Akad. Wetensch.*, ser. B, 55, pp. 212–228.

Weissel, J. K., Lincoln, F. P. and Malinverno, A. (1994). The length–scaling properties of topography. *J. Geophys. Res.*, 99, B7, pp. 13997–14012.

Wewel, F., Scholten, F. and Gwinner, K. (2000). High resolution stereo camera (HRSC) –Multispectral 3D data acquisition and photogrammetric data processing. *Canadian Journal of Remote Sensing*, 26, 5, pp. 466–474.

Wilson, K. G. (1979). Problems in physics with many scales of length. Scientific American, 241, pp. 158–179.

Xu, T., Moore, I. D. and Gallant, J. C. (1993). Fractals, fractal dimensions and landscapes– a review. *Geomorphology*, 8, pp. 245–262.